Journal of South American Earth Sciences
May 2024, Volume 137 Pages 104821 (27p.)
https://doi.org/10.1016/j.jsames.2024.104821
https://archimer.ifremer.fr/doc/00879/99101/

From São Francisco Craton to Jacuipe basin, passing trough the South Tucano and Recôncavo grabens: New insights from wide-angle-MCS data

Aslanian Daniel [1, *], Gallais Flora [1], Evain Mikael [1], Schnurle Philippe [1], Pinheiro Joao Marcelo [1], Afilhado Alexandra [2, 3], Loureiro Afonso [2, 3, 4], Dias Nuno [2, 3], Cupertino J.A. [5], Viana Adriano [5], Moulin Maryline [1]

[1] Geo-Ocean, Univ Brest, CNRS, Ifremer, UMR6538, F-29280, Plouzane, France
[2] IDL – Instituto Dom Luiz, Lisbon, Portugal
[3] ISEL – Instituto Superior de Engenharia de Lisboa, Portugal
[4] FCT – Fundação para a Ciência e Tecnologia, Portugal
[5] Petrobras S.A., Research Center, CENPES, PROFEX, Rio de Janeiro, Brazil

* Corresponding author : Daniel Aslanian, email address : aslanian@ifremer.fr

Abstract :

The structure and nature of the crust underlying the Northeast Brazilian margins have been investigated based on the interpretation of 12 wide-angle seismic profiles acquired during the SALSA (Sergipe ALagoas Seismic Acquisition) experiment in 2014. In this study, we present the coincident analyses of 2 marine seismic reflection and refraction data, SL07 and SL 08, that have been acquired using 15 and 13 ocean-bottom-seismometers along each profile, offshore the Jacuipe Basin. The SL07 has a 270-km long inland continuation with 46 land-seismic-stations crossing the South Tucano and Reconcavo Basins. Wide-angle seismic forward modellings reveal a narrow necking zone, an intermediate domain with anomalously high crustal velocities interpreted as intruded lower continental crust, and a sharp continent to ocean transition zone, greatly different from the adjacent segments (see companion paper of Evain et al.,). Below the Tucano half-grabens, the Moho shows no rise, displaying a flat reflector throughout the landward part of the profile. The high seismic velocities areas in the lower continental crust are interpreted as intrusions that provide an overloading allowing the necessary subsidence for the deposition of the thick sedimentary sequences. Together with the recent information obtained by the analysis of continental basins and aborted rifts, and similar wide-angle experiments on other margins and geodynamic contexts, we propose new paradigm for the thinning process which confirms the crucial role of the lower continental crust and its relation with the upper mantle. We postulate a phase of overloading of the lower continental crust, an exhumation phase of the lower continental crust, and a phase of proto-oceanic crust which involved the lower continental crust and the upper mantle, before the emplacement of a more typical oceanic crust.

Highlights

► This study is part of the SALSA project (**S**ergipe **AL**agoas **S**eismic **A**cquisition), led by IFREMER (France) and Petrobras (Brazil). ► This article focuses on two E-W profiles offshore the Jacuipe Basin, crossing onland the South Tucano and Reconcavo Basin. ► Below Tucano half-grabbens, the moho shows no rise, displaying a flat reflector throughout the landward part of the profile. ► Offshore, a strong E-W-segmentation is described with a very abrupt thinning and a sharp continent ocean-boundary, greatly different from the adjacent segments ► The intermediate domain has anomalously high crustal velocities ans is interpreted as intruded lower continental crust. ► The lower continental crust and its interactions with the mantle play a crucial role, giving rise to a new paradigm. ► 3 phases implying the lower continental crust are described : overloading and subsidence, exhumation, proto-oceanic crust.

1-Introduction

The passive margins are only one part of a system that includes the unthinned continental crusts, its tectonic and geodynamic inheritage, and the oceanic crust, since its birth and first emplacement episodes to its subsequent evolution through time.. For many years, studies have been conducted in a disconnected manner between land and sea. However, understanding the genesis of the passive margins cannot be disconnected from the study of the continental structure from which it originates, nor the sedimentary record that accompanies its evolution. Moreover, as already noticed by Aslanian et al. (2009), no margin presents all the features needed to support the building of a common model of passive margin evolution, but each margin supplies pieces of the jigsaw. This could only be done by comparing many different margins.

We now know that the first oceanic crust has strong affinities with the so-called transitional crustal domain and the lower continental crust, which blurs previously accepted ideas (Aslanian et al., 2009; Evain et al., 2015; Moulin et al., 2015; Afilhado et al., 2015; Aslanian et al., 2021; Moulin et al., 2021, Becel et al., 2020: Loureiro et al., 2023) The vertical motions themselves (subsidence, rebound) do not seem to react as proposed by simple models and the apex of subsidence seems to be delayed after the creation of oceanic crust (Moulin et al., 2005; Aslanian et al., 2009; Labails et al., 2009; Péron-Pinvidic & Manatschal, 2008; Bache et al., 2010; Rabineau et al., 2014; Leroux et al., 2015). Vertical motions leading to large sedimentary gaps are observed and probably linked to an exhumation phase (Aslanian et al., 2009). The role of magmatism and structural inheritance is still poorly understood, and general 3D studies, coupled with more precise 2D studies, are needed. The SALSA experiment, conducted in 2014 by the Department of Marine Geosciences (IFREMER: Institut Français de Recherche pour l'Exploitation de la MER, France) and PETROBRAS (Brazil), in collaboration with the Laboratory of Oceanic Domain (IUEM: Institut Universitaire et Européen de la Mer, France), the Faculdade de Ciências da Universidade de Lisboa (IDL, Portugal) and the Universidade de Brasilia (Brazil), aimed at constraining the crustal structure, the segmentation, and the geodynamical setting of the Jequitinhonha-Almada-Camamu-Jacuípe-Sergipe-Alagoas margin segments. In the year 2000s high quality seismic profiles from ION-GXT were acquired off Brazil's coast (e.g., Kumar et al., 2012). Some of these profiles have been published, particularly in the Brazilian southeastern margin (e.g., Henry et al., 2009; Kumar et al., 2012 ; Romito & Mann, 2021). The location of the SALSA profiles follows some of the ION-GXT profiles.

Seismic shots, Multi-Channel Seismic (MCS) acquisition and Ocean Bottom Seismometers (OBS) deployments were performed by the French R/V L'Atalante (IFREMER) along twelve profiles (Figure 1). Here, we present the results on P-wave velocity models, based on the combined interpretation of multi-channel and wide-angle seismic data, of two profiles imaging the Jacuipe basin (JB). These profiles extended onshore from until the São Francisco Craton, passing trough the South Tucano and Recôncavo grabens. This study contributes to a better understanding of the NE Brazilian margins and completed the already published Almada and Sergipe-Alagoas basins (Loureiro et al., 2018 ; Pinheiro et al., 2018), Camamu and Alagoas basins will be discussed in companion papers (Loureiro, et al., 2023; Evain et al., 2023; Schnurle et al., 2023; Goncalves et al., 2023).

Together with the information given by continental basins and similar wide-angle experiments on other margins and geodynamic contexts (Mediterranean Sea, Central Atlantic Margins, South Atlantic Margins and West Indian Ocean Margins), we can now propose a new and coherent model of passive margin evolution.

2-Geological settings

The distension within Pangea started in the Trias with the separation between the Gondwana and the Laurentia at Late Sinemurian (Sahabi et al., 2004) and a rifting marked by the Central Atlantic Magmatic Province (CAMP), a major igneous eruptions dated about 200 Ma (May, 1971; Bertrand and Westphal, 1977; Marzoli et al., 1999b). Within the Gondwana, the disruption occurred during the early Jurassic (Norton and Sclater, 1979; Patriat et al., 1982; Eagles and Konig, 2008 ; Thompson et al., 2019) coinciding with the Karoo volcanism. During the Early Cretaceous, the break-up of the West Gondwana and the opening of the South Atlantic Ocean was accomplished through lithospheric extension and development of several rift systems, mainly on the Pan-African suture in the south, but also disrupting the E–W segment of the São Francisco–Sangha cratons in the north (Heilbron et al., 2000; Aslanian et al., 2009; Moulin et al., 2010). Some rifts were successful and formed oceanic spreading centres, but others failed and the rift troughs were abandoned at various periods following the jumping of the rift axis to another positions.

In the North-East Brazilian margins, a rift-rift-rift system started at Berriasian/Valanginian Period (Chaboureau et al., 2013), with two NS-oriented branches, the Jequitinhonha-Almada-Camamu margins and the Recôncavo-Tucano-Jatobá (RTJ) onshore rift system. The NE-SW

offshore rift system included the Jacuípe-Sergipe-Alagoas troughs (Chang et al., 1993). By Late Aptian, the NS RTJ onshore rift system was aborted and the drift started in the two other branches (Chaboureau et al., 2013 ; Evain et al., 2023). The connection between the three systems formed the Camamu triple junction, complexifying the geology of the region (Loureiro et al., 2023).

The NS Jequitinhonha - Camamu-Almada was studied in detailed through the combined Wide-Angle (WAS) and Multi Channel Seismic (MCS) analysis in the article of Loureiro et al., 2018. Towards the north, the Alagoas basin was studied in detailed through the combined Wide-Angle (WAS) and Multi Channel Seismic (MCS) analysis in the article of Pinheiro et al., 2018. In this study, we will investigate in the same way the South Tucano and the SW Jacuipe Basins.

Following Milani & Davison (1988), the NS RTJ rift can be regarded as a series of asymmetric half-grabens that are separated by basement highs and a series of NW transfer faults .The transfer faults naturally divide the rift into four sub-basins: Recôncavo, South and Central Tucano, North Tucano and Jatobá, separated respectively by the Apora high, the Itapicuru Transfert Zone, the Vaza-Barris Arch and the Sao Francisco Arch (Figure 1), with the main rift faults dipping eastward in the Northern Tucano and westward in the Recôncavo and South Tucano (Figure 2).

South Tucano and Recôncavo basins seismic images show basement dips consistently towards the southeast (Figure 2A-B). Their main depot-centres are located along the eastern border of the rift system, where the thickness of the non-marine Cretaceous entire sedimentary pile, based on drill wells, can reach 6 km and 4 km in the South Tucano and Recôncavo basins, respectively (Figure 2A-B) (Milani and Davison, 1988). Figure 2C results of a combination of MCS seismic analysis and gravity modelling offshore and pure gravity modelling onshore (Blaich et al., 2008). Below the Tucano and Recôncavo basins, the authors proposed a gently undulating Moho at a depth of 35-30km. New results based on gravity modelling (Alvarez & Holz, 2022) suggest a maximum thickness of circa 16.8 km in the Central Tucano Basin with a Moho interpreted around 24km in the shallower part, suggesting a rise of about 6-8 km relative to the other basins, implying an abrupt crustal necking in the central area, mainly due to the sedimentary basin thickness differences (Figure 2D).

Some P-wave velocity information are also available on the Brazilian Craton. A wide range of continental crustal thicknesses are described for the São Francisco Craton (32 to 50 km) (Assumpção, et al., 2013; Chulick, et al., 2013). The crustal thickness beneath the South Tucano Basin, but also in the Central Tucano Basin, is estimated around 32-36 km (Figure 1-

Assumpção et al., 2013) in contradiction with the value based on gravity modelling (< 10km; Alvarez & Holz, 2022). A P-wave velocity model imaging the South Tucano graben (Oliveira Peixoto, 2013) shows that the sedimentary sequence is about 10km thick and is characterized by velocities of 4.2 km/s (Figures 2E). Below the graben, the modelled crust is composed of 2 layers, with velocities ranging from ~5.5 km/s in the 10 km thick upper continental crust to 6.7-6.9 km/s in the 15 km thick lower continental crust. Along this P-wave velocity profile, the São Francisco Craton is expected to be floored by a 2 layered crust with velocities reaching ~6.2 km/s in the upper continental crust and 6.9-7.0 km/s in the lower continental crust. The Moho lies at 38 km depth (Figure 2E), more in line with the results of Assumpção et al (2013) than those derived from gravity modelling (Alvarez & Holz, 2022). Recently, the analysis of the receiver functions developed at 18 seismic stations in the area reveals that the crust is over 40 km thick beneath the Tucano and Reconcavo basins and that it contains a thick (5-8 km) layer of high velocity (Vs > 4.0 km s(-1)) material below similar to 35 km depth (Döring et al., 2022). Several studies of the North-Eastern Brazilian basin system postulate a pattern of structural inheritance, indicating that pre-existing continental lineaments and transfer zones may exert important influence on the development of these Mesozoic rifting and breakup (e.g. Ussami *et al.*, 1986; Milani & Davison, 1988; Matos 1992; Meyers *et al.*, 1996; Jacques, 2003; Blaich *et al.*, 2008 - Figure 3). Some authors have proposed that SDRs were present on the South Gabon margin (e.g. Jackson et al. 2000), and on the conjugated Brazilian margin, in the Sergipe–Alagoas basin (Mohriak et al. 1995, 1998), suggesting that the central segment of the South Atlantic African margins, to the north of Vaza-Barris transfer zone whoich plaid a crucial rôle in the segmentation of the N-E Brazilian margins (Pinheiro et al., 2018 ; Evain et al., 2023), could also be volcanic. Nevertheless, as pointed out by Moulin et al. (2005) and Aslanian et al. (2009), all seismic images from this central segment are very different from the images obtained on the well-studied volcanic margins. In the Sergipe–Alagoas–Gabon Basins, Ussami et al. (1986), following the lines drawn by Wernicke (1985), proposed a sketch with upper crustal extension onshore and an eastward intra- crustal detachment deeper (see Fig. 3A in Aslanian et al., 2009). On the same profile, Castro (1987) followed the suggestions of Lister et al. (1986) and proposed, a quite opposite sketch with multiple westward detachment surfaces. The problem of the existence of such crustal detachment (or any conservational model), whatever its direction, is the amount of horizontal movement, which is incoherent with the global palinspastic reconstructions (Aslanian et al., 2009; Moulin et al., 2010): as pointed out by Aslanian & Moulin (2012), conservational models are not able to explain all the observations collected in the South Atlantic conjugate Margins together with the palinspastic

reconstructions, the thinning process seems to be depth dependent and to mainly concern the lower/middle crust and it seems not possible that the continental crust would maintain its integrity throughout the thinning process.

Nevertheless, Aslanian *et al.* (2009) pointed out that the presence of two sag basins in the central segment of the South Atlantic Ocean, with an extension of about half of the observed wavelength on the oceanic ridge (Cazenave *et al.*, 1992; Vlastelic *et al.*, 2000; Ondréas *et al.*, 2001), may suggest a correlation between the type of morphology of the passive margins and the thermal segmentation of the upper mantle, in addition to the tectonic heritage and the general thinning process (Aslanian *et al.*, 2009). The striking coincidence between the location of the Bahia Seamounts, with U/Pb ages from 75 to 84 Ma (Skolotonev et al., 2012) and the Margins segment north to the Vaza-Barris transfer zone may show the connexion between the tectonic heritage and the passive margin segmentation and evolution and the upper mantle temperature segmentation (Evain et al., 2023).

Understanding the role and the weight of each parameter implies an analysis of the segmentation from the basins on land to the deep oceanic realms and their possible connections.

3-Seismic acquisition and processing

The SALSA experiment was conducted onboard the *R/V l'Atalante* from April 4th to May 24th 2014. Twelve coincident wide-angle seismic (WAS) and Multi-Channel Seismic (MCS - 360 traces) profiles were collected with 219 deployments of Ocean Bottom Seismometers (OBS) from Ifremer's Marine Geosciences pool (Auffret et al., 2004), as well as additional data of gravimetry, magnetism, bathymetry, sub-bottom and water column (Aslanian et al., 2014). Simultaneously, Land Seismic Stations (LSS) were deployed along the Northeast Brazilian coast, extending five of those profiles on land for about 100 km in order to provide information on the onshore-offshore transition (Figure 1). The seismic source was composed of 15 airguns providing a total volume of 6550-in^3, with a shot interval set at 60 s. Along SL07 and SL08 profiles presented here, a total of respectively 951 and 1189 air-gun shots were generated and recorded jointly by OBS, LSS and a marine 360-channels streamer 4.5 km in length. 12 OBSs spaced every ~12.5 km were deployed along the 170 km long NW-SE oriented SL07 profile, at water depths of 2300 to 4175 m, with the loss of instrument SL07OBS08. 50 km northwards and parallel to the SL07, SL08 is 180km long profile, covered by 13 OBSs at water depths of 2650 to 4195 m. Both profiles cross profile SL06 (Figure 1), which runs parallel to the coast, between 50 km and 100 km from the coastline (Evain et al., 2023). Profile SL07 was extended

onshore with 46 seismometers (Reftek 125A-01 and L-4C) at altitudes ranging from 18 to 459 m, with two stations (SL07LSS13 and SL07LSS1) that recorded only noise. Inter-station distance of 5 km results in a landward extension of this profile of about 270 km. SL07 and SL08 are also almost coincident with portion of industrial ION-GXT2200 and ION-GXT2175 multi-channel seismic profile, respectively (Figures 1 and 4).

MCS Data Processing

SL07 and SL08 profiles were acquired with some problems, mainly due to marine mammal sightings, one loop on each profile was realized. A first quality control and pre-processing was undertaken on the reflection seismic data using the *Solid QC* software (Ifremer), and further processing of the MCS data was then performed using the *GEOCLUSTER* software (CGG Veritas). The processing sequence was composed of geometry, wide bandpass filtering (2-8-64-92 Hz), spherical divergence compensation, deconvolution, Common Mid Point (CMP) sorting, water-bottom multiple attenuation, surface-related multiple modelling and attenuation, editing and water column mute, velocity analysis, Kirchoff pre-stack time migration (PSTM), update of the velocity analysis, normal move-out correction, multiple attenuation in the radon domain, dip move-out, CMP stacking, F-k migration and, Kirchoff post-stack time migration.

Wide-Angle Data Processing

Pre-processing of OBS data included internal clock-drift correction to the GPS base time, and correction of instrument's positions at the seafloor using the direct water wave to take into account the drift during their descent. We applied upward and downward traveling waves separation processing (e.g. Schneider and Backus, 1964) by combining hydrophone and vertical seismometer OBS components. It includes a spiking predictive deconvolution of the upward traveling record using the downward traveling wave to design the filter. Spherical divergence is calculated to compensate amplitude decay of the records and traces are further scaled with a gain proportional to the offset in order to enhance the refracted events.

LSS's records were first debiased and band-pass filtered and stacked by arrays. In addition, the LSS data were reduced by an 8.0 or 8.5 km/s velocity, which flatten the principal Pn arrivals and then processed with an FX deconvolution (in a moving 1.9 s × 21 traces window) to attenuate random noise. A gain equal to the offset was finally applied to enhance the refracted events.

Forward modelling and travel-time inversion

From the seismic data-sets presented above travel-times picks were extracted in order to built a P-wave velocity model along both SL07 and SL08 profiles. We applied an iterative procedure of two-dimensional forward ray-tracing using the RAYINVR software (Zelt and Smith, 1992). Modelling was performed following a layer-stripping strategy, proceeding from top (seafloor) to bottom (Moho and mantle) adjusting for each layer velocity and interface-depth nodes such as to minimize the difference between the observed/picked arrival times and computed ones in the model. Initial models included a water layer where seafloor bathymetry was taken from multibeam data acquired during the SALSA cruise and onshore topography extracted from GEBCO**.** Arrival times of the main sedimentary interfaces up to the acoustic basement were picked from the coincident MCS and ION-GXT lines and integrated in the modelling, as long as they are correlated with identified phases in the OBS data to avoid over-parameterization of the model. We further checked the coherence of our velocity models against MCS data by converting the former from depth to two-way-travel-time (twt). Beyond the acoustic basement, we used only arrival times picked from OBS and LSS records keeping velocity models minimal, i.e. inserting lateral topographic and velocity changes only where required by the data.

Finally, our final models follow a series of tests to assess their validity and reliability. These include statistics on travel-time fits, resolution tests, empirical density conversion and comparison of their calculated gravity signature with the observed one, and pre-stack depth migration of the MCS data based on model's velocities.

SL08 and SL07 final velocity models are composed of 7 sedimentary, 3 and 4 crustal layers (SL08 and SL07 respectively) and 1 mantel layer. One of the crustal layers includes a layer of anomalous high velocity. In the sections below, we explain how these choices were made.

4-Seismic data analysis and velocity model building

Multi-channel Seismic data

The quality of the SALSA MCS data is generally very good, but it decreases beneath the Jacuipe Basin close to the continental slope on both profiles (Figure 5). The modelled sedimentary pile is imaged by a ~2 s twt thick sedimentary sequence and is characterized by numerous pinches out of the sedimentary layers (especially for the layers s3, s4 (SL08) and s5 (SL07) - Figure 5), that are not obvious to interpret on the MCS profile but necessary to explain the refracted arrivals recorded by the wide-angle data. Below these pinch out layers, the seismic facies become almost transparent with only some sparse reflectors imaged on SL07. On the other

hand, the deepest sediments imaged by the SL08 profile are well-stratified and thickening towards the SE in the Oceanic Domain. Strong reflector lying at 6.6 s twt in the Oceanic Domain marks the top of the s5 layer (yellow reflector on Figure 5B). Below the s6 layer is present from 30 to 177 km model distance. The top of the last sedimentary layer s7 is a high amplitude, low frequency, continuous reflector.

Regarding the top of basement, it is difficult to interpret on both MCS data. The layer U (blue interface on Figure 5), is characterized by strong amplitude, disrupted reflectors over a thickness of 0.5 s twt. Its geometry is mainly based on combined interpretation with the coincident ION-GXT lines (Figure 4) and the reflected arrival phases record on OBS. Between 18 and 25 km model distance on SL07, some fan-shaped reflectors can be observed, before a sharp vertical offset of the U Layer towards the ocean.

On Profile SL07 and below the U-Layer of unknown nature, two basement G2 and G3 layers are identified in the Jacuipe Basin based on forward modelling of the OBS ; in the layer B1 is characteristic of the Continental Domain and terminates at the easternmost tip of the necking zone.

On the MCS SALSA07 profile and below the U-Layer of unknown nature, the seismic facies of these basement layers is relatively similar and characterized by an almost transparent facies, except between 10 and 30 km model distance where the G2 layer shows some high amplitude disrupted reflectors (Figure 5A). At depth, a clear high amplitude reflector is present at 6.9 s twt, corresponding to the base of the basement modelled layers. On the MCS SALSA08 profile, the single basement layer G1 is also an almost transparent layer. Although unclear, the Moho interface, marked by few scarce reflectors, seems to lie around 9.5 s twt (SL07) or 9.6 s twt (SL08) (pink reflector on Figure 5B). On both profiles, the deepest layers (BM and M) are mainly interpreted from the seismic wide-angle data.

Wide-angle Seismic data

With respect to OBS and LSS data, the quality is also globally very good. Examples of OBS recorded sections are shown in Figures 6 to 7 while some LSS records are presented in Figure 8 (all OBS and LSS figures can be found in supplementary Figures 1 and 2). Note that the quality of the LSS strongly increases from the LSS deployed in the São Francisco Craton to the LSS deployed closest to the coast in the Salvador high according to the distance from offshore sources of seismic signal. On the LSS deployed on top of the thickest parts of the onshore

sedimentary basins, the signal can be either absent or of very poor quality (e.g. from LSS13 and LSS14). LSS records of offshore seismic shots mostly constrain the necking domain of continental crust but do not allow an estimate of the velocity structure of the crust beneath the Tucano Basin. By chance, we were able to exploit three quarry blasts that were shoot during the SALSA experiment and that were recorded by the SL07LSS (Figures 1 and 9). These were useful information to constrain the geometry of the basement beneath the South Tucano basin and the velocity structure and Moho depth of the continental crust.

Oceanward, the OBS recorded sedimentary refracted events suggest a thick sedimentary succession deposited in the Jacuípe Basin (Figure 6A). Towards the Oceanic Domain, the 7 sedimentary layers identified decrease to 5 layers at the south-eastern end of both profiles (Figure 5). The sedimentary succession presents a continuous trend of increasing velocities from 1.75 (Ps1) to 3.8-4.4 km/s (Ps7) (Figures 6 to 7). Within the first sedimentary layer, no Ps1 refracted arrivals are recorded on the OBS, but the pre-critical reflected Ps2P phase from its base can be clearly identified at near offsets (up to 5 km). According to combined interpretation of the Ps2P and the MCS data, the range of velocities is fixed from 1.75 to 1.80 km/s within the first sedimentary layer on both profiles. The refracted phase from the second sedimentary layer Ps2 is a first arrival and is identified up to 10 km offset, with apparent velocities 2.3 km/s (SL08) or 2.4-2.45 km/s (SL07) (orange refracted phase - Figures 6 to 7).
Generally, SL08OBS records (Figure 6D) are characterized by a fan of second arrival phases with slightly increasing velocities that emerges from the water cone. These second arrivals refracted phases correspond to the deepest sedimentary arrivals Ps3 to Ps7 and are associated with very good record of the associated reflected arrivals Ps2P to Ps7P within the water cone. The reflected arrivals Ps5P and Ps7P are clearly pre-critical arrivals within the water cone on the SL08OBS sections (e.g. yellow (Ps5P) and green (Ps7P) picks on Figure 6B).
On SL07, the top of the s6 layer is marked by a strong Ps6P high-amplitude reflected arrivals recorded at very short offset within the water cone (orange reflector on Figure 7D), the Ps6P corresponds to a very strong reflector on the MCS SALSA07 profile (Figure 5A). The s6 and s7 layers are characterized by velocities ranging from 2.9 to 3.3 km/s. The refracted arrivals Ps6 is extend by the refracted phase Ps7 with a very small velocity contrast at this interface (0.05-0.15 km/s) (Figure 7C towards the SE). The Ps7P reflected phase at the boundary between the layers s7 and s8 is strong amplitude and low frequency reflected arrivals recorded at near offset within the water cone (green reflector on Figure 7D). The deepest sedimentary layer s8 is characterized by the highest velocity within the sedimentary column reaching 3.7-4.0 km/s,

the associated refracted arrival is recorded as a second arrival phase on the wide-angle data (Figure 7D).

In the Jacuipe Basin, the forward modelling of the OBS data was strongly complicated by the roughness of the interfaces below 5 s twt, in particular of the top of basement (Figure 5). Unfortunately, no good constrain of its geometry could be interpreted from both SL07 and SL08 MCS profiles. A strong inclination of top basement interface has strong influence on the ray path of refracted phases propagating within the deepest sediments and basement layers and affects the apparent velocities recorded on the OBS section. To add some constrain on the deep domains where no MCS SALSA data have been acquired – in particular for the geometry of the deep interfaces, we used a combined interpretation between the ION-GXT profiles (Figure 4) and reflected phases recorded on the OBS.

On SL08OBS records, turning waves from the first basement layer arrived at short offset (Pu phase), associated with velocities ranging from 4.7 at the top to 5.6 km/s at the bottom (Figure 6A). No refracted phase Pg1 is registered on the OBS dropped in the Jacuipe Basin. The base of the basement layers is marked by a very clear reflected PuP phase that allows a good constrain on the crustal thickness. A clear strong amplitude first arrival refracted phase Pbm is recorded between 13 and 45 km offset as a first refracted arrival and still at 65 km offset as secondary arrivals (Figure 6A). It is associated with velocities ranging from 7.2 at the top to 7.6 km/s at the bottom. The base of this layer is also marked by a clear and strong reflection PmP observed between 30 and 50 km offset distance. Over the Oceanic domain of SL08 reflected arrivals of wide-angle data, at the base of the U layer are scarce, mainly due to the high-amplitude fan of sedimentary arrivals that mask these pre-critical arrivals. Below, the Pg1 first refracted phase is a clear high amplitude long arrival recorded between ~12 km to 30-35 km (Figure 6), suggesting relatively thick G1 layer. The associated apparent P-velocities of the Pg1 refracted phase are around 7 km/s (Figure 6). The triplication between Pg1, Pn and PmP occurs approximately at an offset of 30-35 km, for all the OBS from SL08OBS11 to SL08OBS01, which indicates an extremely thin crust (Figure 6B-C-D). Pn phases are clearly identified as first and very fast arrivals, having apparent velocity greater than 8 km/s and PmP reflected as on the Moho is registered as long high-amplitude arrivals on the SL08OBS (Figure 6B-C-D). A very deep interface (around 20 km depth) has been inserted in the SL08 P-wave velocity model to better control the gradient of the velocity within the mantle. Some Pn1P reflected arrivals are recorded on this interface at far offset < 35 km.

On SL07 wide-angle data, the Pu arrival phase is very limited in offset and often found within secondary arrivals Reflected arrivals at the base is this layer are sparse and its thickness is constrained by combined interpretation of the OBS and the MCS SALSA07 profile, where the first basement layer is characterized by a chaotic facies (Figure 5B and 7D). Since the G1 layer only extends in the continental domain, the first basement layer is G2. The Pg2 refracted phase shows strong amplitude first arrivals with apparent velocities of 5.2-5.4 km/s (blue refracted arrival - towards the SE on Figure 7 B-C). The deepest high velocity basement layer (G3) is characterized by very long and strong amplitude Pg3 refracted arrivals. It propagates as a first arrival and continues as a second arrival at very far offset reaching 80 km. Its associated velocities range from 6.9 to 7.1 km/s, increasing slightly towards the continent to 7.0-7.2 km/s (Figure 7D). The thickness of this deepest basement layer is well-constrained by the clear high amplitude PmP reflected arrival (Figure 7B and D). The combined interpretation of the MCS SALSA07 profile, SL07LSS records and deep refracted arrivals on SL07OBS suggest that layer G3 pinches out towards the Jacuipe Basin (NW) at 20 km model distance. As for SL08, approaching the Jacuipe Basin, SL07OBS recorded a high velocity refracted first arrival (Pbm) at offset larger than 30 km with associated velocities of 7.55-7.7 km/s (towards the NW pink refracted phase - Figure 7C). On the MCS SALSA07 profile, a strong reflector marked the top of this BM layer that suggest strong crustal thinning (Figure 5A). The base of the BM layer is constrained by a clear and strong PmP observed between 30 and 50 km offset distance on some OBS records (pink reflected phase - Figure 7B-C). Deeper, a low amplitude mantel refracted Pn1 propagates from offsets comprised between 35 to 45 km, with an apparent velocity of 8.0-8.3 km/s (pink refracted phase –Figure 7).

The SL07 profile was prolongated onland with LSS to study the continental structure below the South Tucano and Recôncavo basins. To model the LSS dataset, we gathered the *a priori* information on the geometry of the South Tucano and Recôncavo basins (Milani and Davison, 1988; Mohriak, 2003; Ussami, et al., 1986) and the main known seismic characteristics of the São Francisco Craton surrounding the South Tucano and Recôncavo basins (Assumpção, et al., 2013; Berrocal, et al., 2004; Oliveira Peixoto, 2013; Soares, et al., 2006; Soares, et al., 2010; Tavares, et al., 2012 - see geological context). In addition, we also used three blasts that were shot in a quarry during the SALSA experiment, and that were recorded by the SL07LSS (Figure

9). These provided useful information on the geometry of the base of the South Tucano basin andthe crustal velocity structure of the continental domain.

From the São Francisco Craton to the Aporá high (SL07LSS01 to SL07LSS30), the refracted arrivals from the crust (Pg1 and Pg2) are sparse and recorded as weak to very weak arrivals and no reflected arrivals is recorded at its base. Below the onshore aborted basins, the velocity structure of the continental crust is therefore only constrained by the blast records (Figure 9A) that allowed us to test and adjustour preliminary model (Figure 2).

On blasts records (Figure 9), the first refracted arrival phase Pg1 propagates with an apparent velocities around 6 km/s from 0 to ~135 km offset. It is disrupted by a striking 1 second time shift delay in the Pg1 phase located between 50 and 70 km offset. . These delay marks the possible presence of a major geological feature within the upper continental crust, expected to correspond to the main fault controlling the formation of the South Tucano graben. To explain the time delay recorded by the blasts, we used the head wave propagating at the boundary between the sediments and the basement That way we were able to individualize two major parts of South Tucano graben (Figure 9B):

- one shorter sub-basin located between -210 and -185 km modeled distance: the NW South Tucano Basin,
- a second major sub-basin located between -185 and -120 km modeled distance: the SE South Tucano Basin.

Both grabens show the two main depocenters located at the southeast edge of the basins along NW dipping major faults (Figure 9B). This geometry of the South Tucano graben is in agreement with the available seismic lines acquired across the graben (Figure 2A-B).

A second refracted phase Pg2 and associated reflected phase Pg2P can also be identified on blast records. The Pg2 has apparent velocity above 6.5 km/s. Overall from those blast records we were able to model a two layers (G1 and G2) 37 km thick continental domain with velocity ranges of 6.1-6.25 km/s and 6.5-7.0 km/s respectively.

On LSS records, owing to the very large offset between the stations and the shooting induces that only few arrivals from the Pg1 phase can be identified from SL07LSS01 to SL07LSS30 (see blue refracted phases on supplementary material Figure 2). From SL07LSS31 to SL07LSS46, located further to the SE, below the Aporá high, the Recôncavo Basin and the Salvador high, the Pg1 refracted is recorded as the clear arrival with apparent velocities close to 6.00 (e.g. blue refracted from Figure 8B). A Pg2 refracted phase is also identified on those sections with a slightly higher apparent velocity(e.g. purple refracted arrival on Figure 8B).

LSS records bring valuable information on the deep structure of the continental domain and the necking zone. They allow to constrain the anomalous velocity layer BM already identified on OBS records. A Pbm refracted phase and associated reflected PmP phase are indeed well identified from SL07LSS31 to SL07LSS46. They required is important velocity gradient with the BM layer spanning the necking zone in order to be modeled. From SL07LSS01 to SL07LSS30, a mantel refracted arrival Pn is recorded as a strong amplitude first arrival, until very long offset of 150 km. Similarly, in order to fit Pn travel times, we extended the BM layer below the continental domain, although the velocity range and thickness of the layer cannot be well constrained in this part of the model. Finally, LSS records suggest strong layering within the mantle of the necking zone, particularly based on numerous reflected mantle phase visible on the records. We modeled the strongest one which allowed us to model two mantle layers starting from the necking and extending oceanward with velocities ranging from 8.0 to 8.3 km/s. The modeled continental crust depict therefore in 2 crustal layers, a anomalous BM layer with velocities rangeing from 7.0 to 7.8 km/s, and two mantle layers. Besides the BM layer it is woth to note that our model suggest the Moho is laying flat below the Tucano Basin. .

5-Final models assessment

Travel-times fit

From SL07 and SL08 wide-angle data, we digitized respectively 27834 and 14693 events and interpreted their respective phases (Tables 1 & 2). Travel-time uncertainty was estimated on the SL07 and SL08 OBS records and fixed at 0.030 for the water, 0.050 for the sedimentary arrivals increasing to 0.080 for the crustal and mantelic arrivals for the OBS data. For the SL07LSS, travel-time uncertainty was fixed at 0.200 for all the phases, except for the Pm2P that was fixed at 0.300. SL07 and SL08 final velocity models explain 90% (24998) and 94% (13840) of the travel-time picked, with a global RMS travel-time residual of 0.194 and 0.046, respectively. Given our individual uncertainty, the two models results in a normalized chi-squared of 1.395 for SL07 and 0.671 for SL08 (Tables 3 & 4).

Parametrization and resolution tests

To discuss to accuracy of the final P-wave SL07 and SL08 models, we perform evaluation tests including: hitcount (b), Spread Point Function (SPF) (c) and resolution (d) on Figure 11. This figure presents the four indicators listed below of model quality for SL07 and SL08 profiles, respectively.

For SL07 model, the interface between the upper and lower crustal layers is poorly constrained by reflected arrivals on the LSS records (blue reflected segments on Figure 11A). Towards the ocean, the SL07OBS also did not register reflected phases at the interface between the crustal layers (Figure 11A). To overcome that difficulty during forward modelling, the depth of the crustal interfaces has been fixed to allow rays to propagate within all the crustal layers associated with a correct time predicted time arrival. In contrary the depth of the Moho is very well constrained by the data, especially from -125 to 150 km model distance (Figure 11A). This allows good constrain on the thickness variation of the crust along the SL07 profile. For SL08 profile, at contrary, the deep basement and mantel interfaces are generally well-constrained by reflected arrivals recorded on the wide-angle data (reflected segment on Figure 11E), with 2 exceptions: the base of the B1 layer, and the boundary between the dome-shaped body and the B2 layer. Only few scarce reflected phases are registered in both cases on the wide-angle data. In order to overcome this lack of constrains, we used the MCS profiles SALSA08 and ION-GXT2175 (Figures 4B and 5B).

Regarding the accuracy of the modeled P-wave velocity along the two models, the hit-count is generally low (2500 to 5000) within the upper crust, in the Jacuipe Basin and increases towards the SE in the lower continental crust and the sediments (Figure 11B). The Spread Point Function and the resolution test confirm that the continental structure between -250 and 100 km is poorly resolved, especially in the upper crust with the highest SFP and a resolution comprised between 0.2 and 0.5 (Figure 11C) for SL07. The Spread Point Function (Figure 11G) is good for the whole SL08 model with values around zero, except in the first sedimentary layer and the B2 layer where the SPF reaches 3. Note that generally a resolution matrix diagonals greater than 0.5–0.7 are said to indicate reasonably well-resolved model parameters (Lutter and Nowack, 1990). In that framework most of the SL08 profile, the major part of the interface and velocity nodes present very good resolution (> 0.9) (Figure 11D), except at the NW end of the Jacuipe Basin where only few seismic rays propagate (Figure 11A) and the SL07 profile is well-resolved, except (1) the upper continental crust as discussed before, (2) also the upper crust in the Jacuipe Basin and (3) the velocity at the base of the lens shaped body. For (2), the geometry of acquisition and position of deployment of the OBS (north-westernmost is located at 0 km model distance) explain the small hitcount and the bad resolution of this part of the model. The constraint on the Jacuipe Basin is taken from the interpretation of the both coincident ION-GXT profiles that allows to image the deep geometry (Figure 4). For (3), this result has to be taken into account discussing the origin of the lens-shaped body below the Jacuipe basin, since

it seems that the velocity at the base of this body is poorly constrained by the data (although its thickness is relatively well-constrained – see Figure 11D).

Gravity Modelling

A 2-D gravity model consisting of homogeneous density blocks was constructed from both seismic velocity models: the seismic velocities are converted to densities according to Ludwig et al. (1970), resulting in densities ranging from 2200 to 2950 kg/m^3. The mantle density is set at 3100 kg/m^3 (Figure 12). The modeled free-air anomaly is compared to that observed along the profile.

Free air gravity anomalies extracted along the SL08 profile and along the offshore domain of SL07 present relatively constant values between -10 mGal and -30mGal , except near the continental margin toward the north-west where it decreases up to -80 mGal (Figure 12). The forward model fits reasonably well (within less than 10 mGal) the observed free air anomaly. The worst modeled result are found at the NW end of the profile SL08 where no constrain is available on the geometry of the crust/mantle interface (Figure 11E), that has a strongly influence the gravimetric modeled response.

For the onshore part of the SL07 profile, besides modelling of LSS's arrival time and amplitude, gravity fit needs to be considered in order to verify the consistency of a velocity model with the mass distribution imprint, since P-wave velocity is directly related to density (lithology, rheological properties, fracturing, pore pressure, etc, have a second order contribution to P-wave velocity). Observed free air gravity extracted shows values comprised between -100 and 50 mGal (red points on Figure 12-B). Two strong negative anomalies are present associated with the South Tucano Graben onshore and with the Jacuipe Basin offshore (red point on Figure 12-B). As the forward simplified model presents strong misfits (blue dashed line), it was modified by the addition of heavier density anomalies in the lower continental below the sedimentary basins (Figure 12A) in order to avoid unreasonable load anomalies. The model fits generally well (within less than 30 mGal) the observed trend of free air anomaly (green point on Figure 12-A) especially considering that the continental structure is poorly resolved in the upper crust between -250 and 100 km model distance, as shown by the Spread Point Function and the resolution test. The SL07 model shows a reasonability low load anomalies (less than 200 bar – Figure 12-C) except ibelow the South Tucano Basin. As we do not have sufficient seismic information, we have not tried to improve the fit, but gravity modelling shows that lower crustal density anomalies are required.

Pre-stack depth migration

A Pre-Stack Depth Migrated (PSDM) was performed using the final P-wave velocity model (Figure 13). This allows to discuss the real geometry of the main features imaged by the profiles. The PSDM of the SALSA08 profile strongly improves the seismic imaging of the sediments deposited in the Jacuipe Basin (Figure 13B), showing a rather continuous seismic character with strong well-stratified and high frequency reflectors.

The PSDM of the SALSA07 profile confirms also the homogeneity of the sedimentary succession, composed by well-layered sediments (Figure 13A). On both profiles, high amplitude low frequency continuous reflectors characterized the deepest sediments and the top of the basement is rough lying at 7 km depth in the most oceanward part of both profiles. Comparison between the SALSA model and the line drawing of the depth converted ION-GXT line shows a very good agreement between the layered model on the SALSA models and the main reflectors identified on the ION-GXT profile (Figure 14).

The sedimentary and crustal architecture from the Sao Francisco Craton to the Jacuipe Basin

The final velocity model of profile SL07 (Figure 10A) images the depth geometry of all sedimentary, crustal and mantel layers to a depth of around 70 km. Onshore one sedimentary layer fills the South Tucano grabens with velocities ranging from 2.0-2.2 km/s in the ~3 km thick NW South Tucano sub-basin to 3.7-4.0 km/s in the ~6 km thick SE South Tucano sub-basin. In the Recôncavo graben, the velocities within the sediments range from 4.0 to 4.2 km/s at the base of the basin. The continental crust is 39 km thick and composed of two crustal layers. Below the Tucano Basin to the Recôncavo Basins, the flat Moho is highlighted by interfaces constrained by wide-angle reflections at 38-39km (thick blue lines on Figure 10A). Between –270 and -90 km model distance, the boundary between the upper continental crust and the lower continental crust lies at 20 km deep. Towards the SE this boundary rises over a distance of 40 km, below the Recôncavo graben, to reach 10 km depth at -50 km model distance. The velocities within both the upper and lower continental crusts show some strong lateral variations along the SL07 model. To the NW, characteristic velocities below the São Francisco Craton are 6.3-6.35 km/s in the upper crust and 6.9-7.0 km/s in lower crust. These velocities strongly decrease towards the South Tucano graben to reach 5.7-5.75 km/s in the upper crust and 6.4-6.7 km/s in

the lower crust around -130 km model distance. Further SE, below the Recôncavo graben, the velocities increase to reach 6.1-6.15 km/s in the upper crust and 6.7-6.9 km/s in the lower crust. The crustal necking zone is abrupt and occurs over a distance of less than 40 km. Here the continental crust abruptly thins from 38 km to a very thin 3 km thin crust below the Jacuipe Basin. In this area, the upper crust pinched out around 40 km model distance

Offshore, eight sedimentary layers are modeled with some pinches outs of these layers along the profile SL07. The sediments are 3 km thick and show a continuous trend of increasing velocities from ~1.8 km/s at the seafloor to 3.8-4.1 km/s at the bottom of the sedimentary pile. Between the reflector S8 and the top of the basement, the model presents an about 1 km-thick layer (U-layer), with velocities ranging from 4.7-5.0 km/s below the Jacuipe Basin and increasing oceanward to 5.35-5.5 km/s. However, this layer present two clear disruptions at 30 km model distance, with a vertical offset, and 65 km model distance, with a smaller vertical offset and a difference of rugosity (Figure 5A), which put into question the real continuity of this layer and its associated nature.

On profile SL08, the depth geometry of all sedimentary, crustal and mantel layers are imaged around 20 km depth (Figure 10B). The seven sedimentary layers are characterized by relatively homogeneous P-wave velocities without strong lateral variation. A 5 km thick sedimentary pile is deposited in the Jacuipe Basin whereas only 3 km of sediments covers the oceanward part towards the SE. The P-wave velocities of the sedimentary pile show an increasing trend: the top velocity at the seafloor is 1.75 km/s (s1) and the maximum velocity 4.4 km/s is reached at the base of the sedimentary pile (s7). Some lateral variations in the velocity of the deeper sedimentary layer (s7) are modelled. Here the velocities range from 4-0 to 4.4 km/s below the Jacuipe Basin and decrease oceanwards, towards the southeast to 3.60-3.65 km/s. Between the reflector S7 and the top of the basement, the model shows a layer with velocities increasing towards the ocean from 4.7 km/s (Jacuipe Basin) to 5.2 km/s (SE end of the model), similar to that observed on Profile SL07 (U-layer), with strong rugosity at the toe of the continental slope, although not present on the continetal slope on profile SL08. As on profile SL07, this U-layer presents a disruption at 75km model distance, with a small vertical offset and a difference of rugosity, coincident with a 5 km large basement high observed on the MCS profile (Figure 5B). The continuity and the nature of this layer are also subject of discussion.

Below the U-layer, two layers are modeled on both profiles (Figure 10A-B):

- crust with a thickness of about 5-6 km-between 50 and 180 km model distance is characterized by velocities around 6.60-7.25 km/. This layer thins landwards to 2-3 km in the Jacuipe Basin, between 0 and 50 km model distance
- Below Jacuipe basin, between -10 and 50 km model distance, a lens/dome-shaped is modelled with velocities ranging from 7.55 to 7.7 km/s. On the data, it is associated with a clear reflection on top of the body on the MCS profile (Figure 4B – 5B – 15B) and large offset reflected arrival phases on the OBS records. Its maximum thickness reaches about 5 km, and the structural apex is located below the south-western end of the Jacuipe Basin. The modeled P-wave velocities slightly increases towards the southeast from 7.2-7.6 km/s to 7.3-7.6 km/s.

Between 30km and 150 km model distance, the Moho is clearly imaged by interfaces constrained by wide-angle reflections at 12 km on both profiles; the underlaying layer has typical mantel velocities of 8.0-8.3 km/s. On profile SL08, an intra-mantel reflection lying at 20 km depth (and 50 and 70 km model distance), associated with a reflected Pm2P phase on the wide-angle data. At the base of the SL07 model a deeper layer, with associated velocities of 8.35-8.6 km/s, is distinguished: based on the LSS modelling, a deep intra-mantel reflector lies at 68 km depth below the continent and rises abruptly below the necking zone to reach ~40 km depth.

Discussion

- Nature of Layer U

On both profiles, between the S1-S8 sedimentary reflectors and the basement top (light blue on Figure 5), the MCS data indicate the presence of an about 0.5 sec TWT thick layer U, with some thickening at the toe of the continental slope. The nature and continuity of this layer are unclear. Between 0 and 30km (Profile SL07) and 25km (SL08) model distance, along the continental slope, the layer U presents a transparent facies with chaotic, triangular-shaped geometry on both profiles. At 65 km model distance on profile SL07, and 70 km model distance on profile SL08, the MCS data and the wide-angle model present a small high following by a vertical offset of the U Layer and the basement towards the ocean. Between the toe of the continental slope, at 25-30 km model distance, and these vertical offset, the layer U presents reflective pockets contrasting with the previous transparent facies (Figure 5), indicating that layer U is not a single unit. Towards the sea, the facies of Layer U as well the top of the basement becomes more chaotic.

Layer U is observed on the different profiles of the SALSA experiment. Southwards of Jacuipe basin, on profile SL09, the layer U is proposed as a mixture of salt and sediments in the necking zone, moving to a more volcano-sedimentray layer in Camamu Basin, illustrated by a velocity inversion on the Vz profiles not observed in the necking zone, suggesting the presence a magmatic sublayer in that area (Loureiro et al, 2023). On the perpendicular profile SL06, parallel to the coast and therefore crossing the other SALSA profiles (Figure 1), the continental slope of the Camamu-Jacuipe-Alagoas margin presents the Layer U with a very discontinuous triangular-shaped geometry, interpreted as scattered gravity-slided continental blocks at the toe of the slope (Evain et al., 2023), as described previously in the Gulf of Biscay (Thinon et al., 2003) and the Galicia Bank-Southern Iberia Abyssal Plain strike-slip margin segment (Clark et al., 2007) inside a sedimentary Mass Transport Deposit.
According to those crossing studies, we interpreted the Layer U, in both profiles SL07 and SL08, as a non single unit: a gravity-slided continental blocks inside a sedimentary Mass Transport Deposit (MTD) in the necking zone. The unit evolves into a sedimentary deposit in the Jacuipe basin between 25-30 km and 65-70km model distance, and a crustal layer after the Jacuipe Basin (see Vz below).

In order to characterize the P-wave seismic velocity variations along the two profiles and therefore the nature of the substratum, 1-D velocity-depth profiles were extracted from the velocity model at 10 km interval (Figure 14), from -220 to 140 km (SL07) and 20 to 160 km (SL08) model-distance, respectively where both models are well constrained by seismic ray and well resolved (Figures 10 and 11). We identify four main areas from northwest to southeast: the Continental Domain (including the São Francisco Craton, the South Tucano Basin, the Aporá High, the Recôncavo Basin and the Salvador High) and the Necking Domain exclusively on SL07 profile, the Jacuipe Basin and then the Oceanic Domain on both profiles (Figure 14A-B).

The continental crust is 37 km thick composed of 2 layers with low gradients. The comparison of the 1D velocity profiles with a worldwide compilation of the continental crust (Christensen and Mooney, 1995) clearly shows similarities both in velocities and gradients (Figure 14C). A small step marks the transition between the upper and lower continental crusts at ~19 km depth (Figure 14C). A second step at 37km marks the transition to a 8km-thick layer that presents a range of velocities between 7.5 and 7.7km/s, possibly corresponding to altered or serpentinized

mantle. The results obtained for the structure and thickness of the continental crust of the continental margin are in agreement with a recent compilation of seismic data (Assumpção, et al., 2013) and previous refraction seismic study (Oliveira Peixoto, 2013). NW of the SL07 model, a 39 km-thick continental crust has been interpreted (Assumpção, et al., 2013). The velocities within both the upper and lower continental crusts show some strong lateral variations along the SL07 model. The gravity modelling suggests the existence of positive density anomalies in the lower continental below the sedimentary basin.

We propose that the lower part of the continental crust was overloaded by mafic intrusions, inducing subsidence and the formation of the South Tucano basins (Figures 12 and 16). This model has been proposed for other basins, such as the Parnaïba basin (Tozer et al., 2017; Daly et al., 2018), below the Varanger Peninsula, and the Fedynsky High in the Barents Sea (Shulgin et al., 2018), the Baikal Lake (Thybo and Nielsen, 2009) and the Naval Valley (Moulin et al., 2020; Leprêtre et al., 2021; Schnurle et al., 2023)..

In the Necking Domain, the thick continental crust thins abruptly over a distance of less than 50 km: the top of the basement deepens from 0 to 5 km, whilst the Moho rises from 40 km to ~15 km SW (Figure 14D & 16). South-eastwards, the upper continental layer pinches out and disappears in the Jacuipe Basin, leaving place to a very thin crust. Beneath the Jacuipe Basin, a lens/dome shaped layer presents characteristic velocities of 7.55-7.7 km/s (SL07) or ~7.25 to 7.6 km/s (SL08), with a maximum thickness of 5/7 km (on SL08 and SL07 respectively). This layer BM (for Basement-Mantle) pinches out towards the SE (Figures 10 and 14), that termination is well-constrained as attested by the resolution test (Figure 11A-E). The 1-D velocity-depth profiles beneath the Jacuipe Basin do not fit the 1-D velocity-depth profiles compiled for the Atlantic Ocean (Christenson et al., 2019), excluding an oceanic nature of the basement (Figure 14-E) but are similar to the 1-D velocity-depth profiles in the Para-Maranhão-Barreirinhas Margin, North Brazil, (Figure 17) interpreted as an exhumed lower continental crust above a High Velocity Layer, possibly corresponding to intruded continental crust and/or altered or serpentinized mantle (Aslanian et al., 2021). Above and along the continental slope and at its toe, the composite U-layer of MTD and few Triangular-shaped gravity-slided continental blocks, as described in Galicia Bank-Southern Iberia Abyssal Plain strike-slip margin segment (Clark et al., 2007), is probably connected to the strike-slipe movement of the multiphase kinematic evolution of the Camamu/Jacuipe-Sergipe-Alagoas segment (Evain et al., 2023). This layer continues towards the ocean in the Jacuipe Basin, moving to a more sedimentary unit.

Further SE, after the topographic high between 65 and 75 km model distance, the Domain is characterized by a homogeneous velocity structure within the upper oceanic crust of 5.4-5.6 km/s, within the middle oceanic crust of 6.2 to 6.7 km/s and within the lower oceanic crust 6.9-7.1 km/s in three layers on SL07 profile. On SL08 profile, two layers are interpreted, one within the upper crust (~5.3 to ~5.7 km/s) and the other within the lower crust (~6.5 to 7.2 km/s) (Figure 14F). The thickness of the basement is 6 km, corresponding to a Moho interface at 13 km depth, coherent with the interpretation of the ION GXT profiles (Figures 4 and 15). At the base of both models, no strong variation of the Vp velocity within the mantle is observed: the mantle, which appears to be altered/serpentinised further to the north-east in an 5 km thick upper layer (velocity around 7.5-7.7 km/s), is constant here around 8.0 to 8.3 km/s (Figure 14E-F). The 1-D velocity-depth profiles of this domain are in good agreement with the compilation of Atlantic oceanic crusts of similar age (White et al., 1992) and a compilation of oceanic crusts (Christesonn et al., 2019) (Figure 14).

Conclusions

From the wide-angle observations, the SL07 and SL08 models highlight three striking features (Figure 16):

- onshore, presence or absence of the rifted basins has no influence on the deep crustal structure. The Moho is flat and lies at a constant depth comprised between 35 to 38 km depth. Together, wide-angle, isostasy and gravity modelling suggest the presence of intrusions in the lower continental crust that provide an overloading allowing the necessary subsidence in the aborted sedimentary basins. The maximum thickness of sediments within the basins is 6 km.
- offshore, the necking is very sharp, with some small gravity-slided continental blocks at the toe of the slope, inside a Mass Transport Deposit, probably connected to the strike-slip phase of the kinematic evolution of the margin.
- the transitional domain, before a typical oceanic domain, is narrow and presents velocity structure coherent with exhumed continental crust above an intruded continental crust and/or an altered or serpentinized mantle (Evain et al., 2023).

Passive continental margins are very diverse in geometry, nature and evolution; this diversity may be a matter of tectonic heritage, geodynamic context and mantle temperature and an unique

thinning process can be questioned. It is unreasonable to try to build this common thinning model, if it exists, on the observation of a single margin: as quoted 14 years ago (Aslanian et al., 2009), the difficulty is to decipher between local (which probably produce the diversity of the margins) and general characteristics. This could only be done by comparing many different margins, using if possible the same methodology implying dense and crossed wide-angle and MCS profiles (to avoid over-interpretation and to take into account possible lateral variations), magnetism, gravity and isostatic modelling and independent precise kinematic studies. Note that the use of wide-angle data is indispensable to well-constrain deep structure and avoid over interpretation of the MCS data (Loureiro et al., 2018).

Some common, essential and unavoidable features should be highlighted, which break with the ideas that have more or less prevailed for almost 40 years:

1 There are few evidence for large extensional faults. With some rare exceptions, due to a particular geodynamic context, very few tilted continental blocks can be observed, some of them being probably produced by gravity-sliding (Thinon et al., 2003 ; Clark et al., 2007; Evain et al., 2023).

2 The system is in high position, close or above the sea level, all along its genesis and at least until the break-up (for instance, Dupré et al., 2007, Péron-Pinvidic & Manatschal, 2008; Aslanian et al., 2009).

3 The necking zone is rather narrow in many margins, meaning a quite abrupt thinning of the crustal layers

4 The more or less large transitional domain is mainly of exhumed middle/lower continental crust showing its crucial role in the genesis of the passive margin at least on the Angola Margin (Contrucci et al., 2004 ; Moulin et al., 2005 ; Aslanian et al, 2009), in the Mediterranean sea (Moulin et al., 2015; Afilhado et al., 2015), the Equatorial Atlantic (Aslanian et al., 2021; Moulin et al., 2021; Schnurle et al. 2023, Aslanian & Moulin, 2012), Santos Basin (Evain et al., 2015; Moulin et al., 2012), the Jequitinhonha-Almada-Camamu-Sergipe-Alagoas Margins (Loureiro et al., 2018; Pinheiro et al., 2018; Loureiro et al., 2023; Evain et al., 2023), the North Colorado margin (Shuck et al., 2019; Becel et al., 2020), and even on the so-called volcanic margins :NW Greenland margins (Guan *et al.,* 2019), the margins of the austral segment of the South Atlantic ocean (Chauvet et al., 2021, Geoffroy et al., 2022).

5 As suggested in the early 70's (Bott, 1971) the lower continental crust may flow and gradually recrystallize to build a first proto-oceanic oceanic crust (Bott, 1971; Aslanian et al., 2009; Sibuet et al., 2012; Afilhado et al., 2015; Aslanian et al., 2021; Moulin et al., 2021), leading to complete continental mantle erosion before the first typical oceanic crust appears (Bécel et al., 2020).

6 As shown previously in the south Atlantic margins (Aslanian et al., 2009 ; Aslanian & Moulin, 2012), the precise palinspastic reconstruction of the systems show that the horizontal movements of the plates can generate only a small part of the thinning process and some of the middle/lower crust disappears : it seems most improbable that the continental crust would maintain its integrity throughout the thinning process and interaction may occur with the upper mantle underneath. These points are far from being inconceivable if we keep in mind that continental break-up nearly always occurs inside previous orogenic belts and that the material involved in the process is therefore highly heterogeneous.

The results in the Tucano Basin present a flat Moho discontinuity that lies at a constant depth around 37 km with the presence of intrusions in the lower continental crust, providing an overloading that induced subsidence in the aborted sedimentary basins. Similar results and conclusions, based on wide-angle and MCS seismic data, were shown and proposed in continental basins or aborted rift as in the Baikal Lake (Thybo and Nielsen, 2009), the Parnaíba cratonic basin (Tozer et al., 2017) or the Mendeleev Rise and the Chukchi Plateau in the Arctic Ocean (Kashubin et al., 2018) and the Natal Valley, south of the Mozambique Coastal Plain in the Indian Ocean (Moulin et al., 2020; Lepretre et al., 2021 ; Evain et al., 2021; Aslanian et al., 2021; Schnurle et al., 2023; Moulin et al., 2023).

All these results complete and precise the geodynamic evolution (Figure 18) that we proposed fourteen years ago (Aslanian et al., 2009), implying a first phase of overloading of the continental crust by mantle intrusions or mineral phase transformations, producing subsidence and sedimentary deposition as suggested by Tozer et al. (2017).

This phase may abort as in the continental basins mentioned above (Fig 18-A) or in the Natal Valley and the Mendeleev Ridge (Figure 18-B). In the passive margins, this intrusion phase is followed by an exhumation phase (first breakup). McKenzie et al. (2000) show that magmatic activity can reduce the viscosity of the lower crust to a level that allows flow, thus producing the intermediate crust domain observed on the wide-angle seismic data (Figure 18-C). While in

the so-called non-volcanic margins subsidence produces a thick sedimentary basin in the intermediate domain, in the so-called volcanic margins this exhumation phase is accompanied by the development of seaward dipping reflectors as described on the Greenland margins or on the South-Austral Atlantic margins. While these SRDs have been recognized as a ubiquitous feature of this type of margin, the subject of the nature of the underlying crust is contentious: while Paton et al. (2017) described the crust containing the SDRs having similarities to oceanic crust, McDermott et al. (2018) interpreted the transition from Type I to Type II SDRs as a continuum from continental rifting to full plate separation with formation of new, subaerially generated, magmatic crust. More recent studies (Chauvet et al., 2021; Geoffroy et al., 2023) suggested that the underlying crust shares few of the characteristics of oceanic crust and proposed instead that "*the middle-lower continental crust could be exhumed and made brittle at the most distal end of volcanic passive margins".* This exhumation phase ends either by the emplacement of a proto-oceanic crust, fed by continental crust as earlier suggested by Bott (1971), or in some case in more typical oceanic crust (Figure 18-D).

This model therefore proposes a new paradigm for the thinning process which confirms the crucial role of the lower continental crust and its relation with the upper mantle, with a phase of overloading of the lower continental crust, aa exhumation phase of the lower continental crust and a phase of proto-oceanic crust which involved the lower continental crust and the upper mantle, before a more typical oceanic crust.

Acknowledgements:

The data set collected during the SALSA experiment is protected under a partnership between IFREMER and Petrobras. Any request has to be addressed to Daniel Aslanian (aslanian@ifremer.fr) and Adriano Viana (avaina@petrobras.com.br). The authors wish to thank the captain, crew, and MCS technical team of the French R/V L'Atalante. Many thanks also to the OBS and land station technical teams who made this experiment possible. The authors acknowledge financial support from CAPES-COFECUB. The authors acknowledge the fruitful and constructive comments by Webster Mohriak and another anonymous reviewer, which greatly improved the manuscript.

The GMT [Wessel and Smith, 1998], Seismic Unix package [Stockwell, 1999], GEOCLUS-TER (CGG-Veritas), and RAYINVR (Zelt and Smith, 1992; Zelt et al., 1999) softwares were used in the preparation of this paper.

Contributions

The SALSA Project was imagined and led by D. Aslanian and M. Moulin and led by D. Aslanian and M. Moulin from Ifremer and A. Viana, Jose A Cupertino from Petrobras. The Onshore part of the project was managed by N. Dias and A. Loureiro from ISEL (Lisbon), R. Fuck and J. Soares from University of Brasilia. Modelling of the SALSA profiles was done by A. Afilhado, M. Evain, F. Gallais, F. Klingeklhoefer, A. Loureiro, M. Moulin, J. Pinheiro, and P. Schnurle. Processing of the deep seismic reflection data was done by P. Schnurle. Landstantions were deployed by N. A. Dias, A. Afilhado, A. Loureiro, C. Corela. The Geologic interpretation interpretation were done by D. Aslanian, M. Moulin., P. Schnürle, A. M. Evain, F. Gallais, A. Loureiro, J. Pinheiro,. All co-authors participate to the writing of the paper. In addition to the co-authors, the SALSA Team was composed by: D. Alves, A. Baltzer, P. Barros Junior, M. Benabdelhouahed, Y. Biari, C. Corela, J. Crozon, J.L. Duarte, C. Ducatel, C. Falcão, P. Fernagu, D., Le Piver, J.P. Mazé, Z. Mokkedem, L. Morvan, P. Pelleau, D. Pierre, M. Rabineau, C. Rigoti, I. Rio, M. Roudaut, M. Roudaut-Pitel, & W. Roest

Figures caption:

Figure 1: Location of the SL08 and SL7 profiles, respect to others SALSA and ION-GXT dataset on topographic map derived from satellite data (Sandwell & Smith, 1997). Compilation of avalaible information on geology of the onshore Tucano and Reconcavo Basins from Ussami et al., 1986; Milani and Davison, 1988; Mohriak, 2003, Blaich et al., 2008; Assumpçao et al., 2013 and Oliveira Peixoto, 2013. Previous studies from SALSA datasets (Pinheiro et al., 2018, Loureiro et al., 2018) are also indicated by a red and blue square, respectively.

Figure 2: Compilation of available information on the geology of the onshore Tucano and Recôncavo Basins from Ussami et al., 1986; Milani & Davison, 1988; Mohriak, 2003; Blaich et al., 2008; Assumpção et al., 2013 and Oliveira Peixoto, Pers. Comm.. Onshore morphology of the South Tucano and Recôncavo Basins: A- Two-travel time (s) seismic section after Mohriak, 2003; B- Depth seismic section after Milani and Davison, 1988. C- Gravity modelled transect from Tucano to Jacuipe Basin (Blaich et al., 2008), D- Gravity modelled transect from Tucano to Jacuipe Basin (Alvarez & Holz, 2022) ; E) Preliminary a priori model for the SL07LSS wide angle data modelling based on a compilation of published and unpublished data. F- Location of the different profiles..

Figure 3: Modified from Aslanian et al., 2009. Left Three schematic cross-sections in NE Brazil and N Gabon (See localisation in Fig 1 and in the right insert) based on gravity data, and three hypotheses. A) The hypothesis of Ussami et al. (1986) follows the lines suggested by Wernicke (1985) with an upper crustal extension onshore and intra-crustal detachment deeper. Note that the detachment dips eastwards and therefore the upper plate is on the Gabonese side. B) The hypothesis of Castro (1987), based on the

combination of profiles 2 and 2′, follows the suggestions of Lister et al. (1986), with multiple detachment surfaces. Note that in this case the detachments dip westwards and therefore the upper plate is on the Brazilian side. C) The hypothesis of Blaich (2006), a combination of the previous two. Right insert: location of the profiles. South America is fixed. Africa is in its position at 112 Ma after Moulin (2003). Note that in this reconstruction, the conjugate margin of the Reconcavo–South Alagoas–Jequitinhonha margin system is the south Gabon margin. Previous work on Sergipe–Alagoas Basin (Meyers et al., 1996; Castro, 1997; Mohriak and Rosendahl, 2003…) have used kinematic reconstructions, in which the conjugate margin of the north of Sergipe–Alagoas margin was the oblique transform Rio Muni Margin. These reconstructions present a shift of more than 150 km for the Ascension FZ (Aslanian et al., 2009) and cannot be used to define the conjugate margin. Maximum sediment thickness areas come from Brink (1974), Cordani et al. (1984) and Lana (1985), in Castro (1987).

Figure 4: Line drawing of the Pre-Stack Depth Migration sections of the ION-GXT 2200 (equivalent to SL07) and ION-GXT 2175 (equivalent to SL08) overlain by interfaces of wide-angle models. The intersections with the SALSA dataset are indicated by blue line. Vertical exaggeration at seafloor is 1:2.

Figure 5: Insert of SALSA dataset (blue lines), SL07 and SL08 profiles are indicated by red lines. OBS and LSS locations are indicated by white circles. Two-way travel-time record section of MCS data along SALSA 07 (A) and SALSA08 (B) profiles overlain by time converted interfaces of wide-angle model. The intersections with the SALSA dataset are indicated by red line. OBS location are indicated by black triangle. Vertical exaggeration at seafloor is 1:12.5.

Figure 6: A) SL08OBS13 on profile SL08 – northwest direction to the right and southeast to the left. a) Seismic record; b) Synthetic; c) Color coded synthetic; d) Color-coded observed travel-times overlain by predicted times in black; e) Seismic rays; f) MCS time migrated section and colour-coded model interfaces. On a, b, c, and d, travel-time is reduced by a velocity of 7 km/s. B) SL08OBS09 on profile SL08 – same legend than A. C) SL08OBS07 on profile SL08 — same legend than A D) SL08OBS02 on profile SL08 – same legend than A.

Figure 7: A) SL07OBS02 on profile SALSA07 – southeast direction to the right and northwest to the left. a) Seismic record; b) Synthetic; c) Color coded synthetic; d) Color coded observed travel-times overlain by predicted times in black; e) Seismic rays; f) MCS time migrated section and color-coded model interfaces. On a, b, c, and d, travel-time is reduced by a velocity of 7 km/s. B) SL07OBS05 on profile SALSA07 – same legend than A, C) SL07OBS06 on profile SALSA07 – same legend than A. D) SL07OBS12 on profile SALSA07 – same legend than A.

Figure 8: A) SL07LSS08 on profile SL07 on the São Francisco Craton. a) Seismic record; b) Synthetics; c) Color coded synthetics; d) Color-coded observed travel-times overlain by predicted times in black; e) Seismic rays. On a, b, c, and d travel-time is reduced by a velocity of 8 km/s. B) SL07LSS35 on profile SL07 on the Recôncavo graben. Same legend than A.

Figure 9: Three quarry blasts detected during the SALSA experiment, their extracted travel times superposed on seismic traces (a,d,g), the fit (b,e,h) and ray tracing (c,f,i) obtained in SL07 final velocity model. Position of blasts are indicated by red dots on inset maps and recording SL07LSS by a thick black line. Color coded picks are as in figure 6A

Figure 10: Final P-wave interval velocity models along SL08 and SL07 profiles. OBS and LSS locations are indicated by white circles. Inverted black triangle mark OBS positions. Thin blue lines mark the intersections with the SALSA dataset. Black lines mark model layer boundaries. Coloured areas are constrained by seismic rays. Thick blue lines indicate interfaces constrained by wide-angle reflections. Vertical exaggeration is 1:2.

Figure 11: Evaluation of the wide-angle models SL08 and SL07. a) Model parameterization includes interface depth nodes (squares), top and bottom layer velocity nodes (red circles); interfaces where reflections have been observed on OBS data are highlighted in blue. b) Hit-count for velocity (gridded and colored) and depth nodes (colored squares). c) Smearing from Spread-Point Function (SPF) for velocity (gridded and colored) and depth nodes (colored squares). d) Resolution of velocity (gridded and colored) and depth nodes (colored squares). Zones that were not imaged are blanked.

Figure 12: Gravity modelling along the SL08 (A) and SL07 (B) models. a) Density model up to a depth of 90 km overlain by interfaces from wide-angle modelling. b) Free-air gravity anomaly observed (Pavlis et al., 2012) along the SL07 model calculated with the wide-angle model (dashed blue line) and calculated with lower crustal anomalies (green line). c) Load anomaly with lower crustal anomalies.

Figure 13: Pre-stack depth migrated record section of MCS data along SALSA07 and SALSA08 profiles. Model's interfaces are represented with continuous lines. The intersections with the SALSA dataset are indicated by red line. Vertical exaggeration is 1:5.

Figure 14: Distribution of 1-D velocity profiles extracted from the final P-wave interval velocity model and color coded according to segmentation along the SL07 and SL08 profiles. (b) P-wave interval velocity as a function of depth below seafloor. (c) P-wave interval velocity as a function of depth below basement. Note that the 1-D velocity profiles are extracted only where the model is constraint by seismic rays.

Figure 15: A- Final P-wave interval velocity model along SL07 and SL08 profiles. Black lines mark model layer boundaries. Colored area is constrained by seismic rays. Inverted black triangle mark OBS positions. Thin blue lines mark the intersections with the SALSA dataset. Vertical exaggeration is 1:2. B- Zoom on the final P-wave interval velocity model along SL07 and SL08 profile superimposed by the interpretation on the ION-GXT2200 and ION-GXT2175 profiles. Vertical exaggeration is 1:2.

Figure 16: Proposition of interpretation.

Figure 17: Comparison between 1-D velocity profiles extracted from the final P-wave interval velocity model in the Jacuipe Basin and 1-D velocity profiles of the exhumed continental crust of Barreinrinhas/Ceara Margins (Aslanian et al., 2021)

Figure 18: Left: Model of sedimentary basin and passive margin genesis in four phases, emphasizing the crucial role of the lower continental crust. Right: some examples for each phase with real data, from the top to bottom after Tozer et al. (2017), Moulin et al. (2020), Moulin et al. (2015), Aslanian et al. (2021). In green font, some published examples of each phase.

Table 1: Reflected or refracted phase name, number of explained events, residual mean-square, and normalized chi-squared value for SL07 profile

Table 2: Reflected or refracted phase name, number of explained events, residual mean-square, and normalized chi-squared value for SL08 profile.

Table 3: Instrument name, distance along model, direction code, number of explained events, residual mean-square, and normalized chi-squared value for SL07 profile.

Table 4: Instrument name, distance along model, direction code, number of explained events, residual mean-square, and normalized chi-squared value for SL08 profile.

References

Afilhado, A. Moulin, M., Aslanian, D., Schnürle, P., Klingelhoefer, F., Rabineau, M., Leroux, E., Beslier, M.-O., (2015). Deep Crustal Structure Across An Young Passive Margin From Wide-Angle And Reflection Seismic Data (The Sardinia Experiment) – II: Sardinia's Margin, *Bulletin de la Société Géologique de France*, 186, n°4-5, 331-351, doi:10.2113/gssgfbull.186.4-5.331

Alvarez, P., & Holz, M., 2022. The Tucano Basin (Cretaceous, Brazil) – a world-class example of an aborted rift system with anomalous depth. Journal of South American Earth Sciences, 119. 103975

Aslanian, D., Moulin, M., Olivet, J.-L., Unternehr, P., Matias, L., Bache, F., Rabineau, M., Nouzé, H., Klingelhoefer, F., Contrucci, I. & Labails, C., 2009. Brazilian and African passive margins of the Central Segment of the South Atlantic Ocean: Kinematic constraints, *Tectonophysics*, *468*, 98–112.

Aslanian, D. & Moulin, M., 2012. Paleogeographic consequences of conservational models in the South Atlantic Ocean, *In*: Mohriak, W.U., Danforth, A., Post, P.J., Brown, D.E., Tari, G.C., Nemcok, M. & Sinha, S.T. (*eds*). Conjugate Divergent Margins. *Geological Society, London, Special Publications*, 369, http://dx.doi.org/10.1144/SP369.5,

Aslanian, M. Moulin, M. Evain, P. Schnürle, F. Klingelhoefer, M. Benabdellouahed, A. Baltzer, F. Gallais, A., Afilhado, Z. Mokeddem, Y. Biari, C. Ducatel, C. Rigoti, C. Falcao, Paulo de Melo Barros Junior, P. Pelleau, J. Crozon, P. Fernagu, M. Roudaut, D. Le Pivert, J. E. Pereira Soares, R., Fuck, N. Dias, J.-L., Duarte, M. Vinicius Aparecido Gomes de Lima, A. Loureiro, D. Alves, C. Corela & L. Matias, 2014. Confidential cruise report and preliminary results of the SALSA Experiment..

Aslanian, D., Gallais, F., Afilhado, A., Schnurle, P., Moulin, M., Evain, M., Dias, N., Soares, J., Fuck, R., da Cruz Pessoa Neto, O., Cupertino, J.A., Viana, A. and the MAGIC Team, 2021. Deep structure of the Pará Maranhão/Barreirinhas passive margin in the Equatorial Atlantic (NE Brazil), *Journal of South American Earth Sciences*, 110, https://doi.org/10.1016/j.jsames.2021.103322

Assumpçao, M., Bianchi, M., Julia, J., Dias, F.L., França, G.S., Nascimento, R., Drouet, S., Pavao, C.G., Albuquerque, D.F., Lopes, A.E., 2013. Crustal thickness map of Brazil: Data compilation and main features, *Journal of South American Earth Sciences*, *43*, 74-85.

Auffret, Y., Pelleau, P., Klingelhoefer, F., Géli, L., Crozon, J., Lin, J.I., Sibuet, J.-C., 2004. MicrOBS : a new generation of bottom seismometer. *First Break*, 22, 41–47.

Bache, F., Olivet, J.-L., Gorini, C., Aslanian, D., Labails, C. & Rabineau, M., 2010. Evolution Of Rifted Continental Margins: The Case of The Gulf of Lions (Western Mediterranean Basin), *Earth And Planetary Science Letters*, 292, 345-356.

Becel, A., Davis, J.K., Shuck, B.D., Van Avendonk, H.J.A., Gibson, J.C., 2020. Evidence for a prolonged continental breakup resulting from slow extension rates at the eastern north American volcanic rifted margin. J. Geophys. Res.: SolidEarth 125. https://doi.org/10.1029/2020JB020093 e2020JB020093.

Berrocal, J., Marangoni, Y., de Sa, N., Fuck, R., Soares, J., Dantas, E., Perosi, F. and Fernandes, C., 2004. Deep seismic refraction and gravity crustal model and tectonic deformation in Tocantins Province, Central Brazil, *Tectonophysics*, *388*, 187– 199.

Blaich, O.A., Tsikalas, F., Faleide, J.I., 2008. Northeastern Brazilian margin: regional tectonic evolution based on integrated analysis of seismic reflection and po- tential field data and modelling. Tectonophysics 458 (1), 51e67. https://doi.org/ 10.1016/J.TECTO.2008.02.011.

Bott, M.H.P., 1971. Evolution of young continental margins and formation of shelf basin. Tectonophysics 11, 319–337.

Brink, A.H., 1974. Petroleum geology of Gabon Basin. American Association of Petroleum Geologists Bulletin 58 (2), 216–235.

Castro Jr., A.C.M., 1987. The northeastern Brazil and Gabon Basins; a double rifting system associated with multiple crustal detachment surfaces. Tectonics 6 (6), 727–738.

Cazenave, A., Houry, S., Lago, B. And Dominh K., 1992. Geosat-Derived Geoid Anomalies At Medium Wave- length, J. Geophys. Res., 97, 7081-7096.

Chaboureau, A.-C., Guillocheau, F. Robin, C., Rohais, S., Moulin, M. & Aslanian, D., 2013. Palaeogeographic evolution of the central segment of the South Atlantic during Early Cretaceous times: palaeotopographic and geodynamic implications, *Tectonophysics*, 604: 191-223, doi:10.1016/j.tecto.2012.08.025

Chauvet, F., Sapin, F., Geoffroy, L., Ringenbach, J.-C., Ferry, J.-N., 2021. Conjugate volcanic passive margins in the austral segment of the South Atlantic – Architecture and development. Earth-Science Reviews, 212. 103461

Christensen, N. I., and D. W. Mooney, 1995. Seismic velocity structure and composition of the continental crust: A global view, *Journal of Geophysical Research*, *100*, 9761-9788.

Christeson, G.L., Goff, J.A., Reece, R.S., 2019. Synthesis of oceanic crustal structure from two-dimensional seismic profiles. *Rev. Geophys.* 57, 504–529. https://doi.org/10.1029/2019RG000641

Chulick, G. S., Detweiler, S. & Mooney, W.D., 2013, Seismic structure of the crust and uppermost mantle of South America and surrounding oceanic basins, *Journal of South American Earth Sciences*, *42*, 260-276.

Clark, SA, Sawyer DS, Austin JA, Christeson, GL, Nakamura Y., 2007. Characterizing the Galicia Bank-Southern Iberia Abyssal Plain rifted margin segment boundary using multichannel seismic and ocean bottom seismometer data. J. Geophys Res., 112,

Cohen, J. and Stockwell, J. J. W., 2019. CWP/SU: Seismic UnxRelease No. 44: an open source software package for seismic research and processing.

Contrucci, I., Matias, L., Moulin, M., Géli, L., Klingelhoeffer, F., Nouzé, H., Aslanian, D., Olivet, J.-L., Sibuet, J.-C., Réhault, J.-P., 2004. The crustal structure of the NW Moroccan continental margin from wide-angle and reflection seismic data, *Geophysical Journal International*, *139*, 117–128.

Cordani, U.G., Neves, B.B.B., Fuck, R.A., Porto, R., Filho, A.T., Cunha, F.M.B., 1984. Estudo preliminar de integraçao do Pre-Cambriano com os eventos tectonicos das bacias sedimentares brasileiras, Serie Cienca-Tecnica-Petroleo Secao: Exploraçao de Petroleo, Publ. 15, 70 pp., PETROBRAS.CENPES.SINTEP, Rio de Janeiro.

Daly, M. C., Fuck, R. A., Julià, J., Macdonald, D. I. M., & Watts, A. B., 2018. Cratonic basin formation: A case study of the Parnaíba Basin of Brazil. *Geological Society, London, Special Publications*, *472*, 1–15. https://doi.org/10.1144/SP472.20

Döring, MF, Julia, J., Evain M. 2022. Joint inversion of receiver functions and surface wave dispersion in the Reconcavo-Tucano basin of NE Brazil: implications for basin formation Geophysical Journal International, Volume 230, Issue 1, Pages 317–333, https://doi.org/10.1093/gji/ggac080

Dupré, S., Bertotti, G. & Cloetingh, S., 2007. Tectonic history along the South Gabon Basin: Anomalous early post-rift subsidence. *Marine and Petroleum Geology*, *24*, 151-172.

Evain, M., Afilhado, A., Rigoti, C., Loureiro, A., Alves, D., Klingelhoefer, F., Schnurle, P., Feld, A., Fuck, R., Soares, J., Vinicius de Lima, M., Corela, C., Matias, L., Benabdellouahed, M., Baltzer, A., Rabineau, M., Viana, A., Moulin, M. & Aslanian, D., 2015. Deep structure of the Santos Basin-São Paulo Plateau System (SSPS), *Geophys. Res. Solid Earth*, 120, doi :10.1002/2014JB011561,

Evain, M., Schnürle, P., Leprêtre, A., Verrier, F., Watremez, L., Thompson, J.O., De Clarens, P., Aslanian, D. and Moulin, M., 2021. Crustal structure of the East African Limpopo margin, a strike-slip rifted corridor along the continental Mozambique Coastal Plain and North Natal Valley, *Solid-Earth*, 12, 1865–1897, https://doi.org/10.5194/se-12-1865-2021.

Evain, M., Schnürle, P., Gallais, F., Pinheiro, J.M., Afilhado, A., Loureiro, A., Klingelhoefer, F., Dias, N., Cupertino, J.A., Viana, A., Aslanian, D. and Moulin, M., Along strike segmentation of the northeastern Brazilian margins: the role of inherited lithospheric structures and kinematics, *Journal of South American Earth Sciences*, 128, 104479 (20p.). *https://doi.org/10.1016/j.jsames.2023.104479*

Geoffroy, L., Chauvet, F. & Ringenbach, JC. 2022. Middle-lower continental crust exhumed at the distal edges of volcanic passive margins. Commun Earth Environ 3, 95. https://doi.org/10.1038/s43247-022-00420-x

Gonçalves, S., Schnürle, P., Rabineau, M., Afilhado, A., Aslanian, D., Evian, M., Moulin, M., Loureiro, A., Dias, N., Deep crustal structures with Reverse Time Migration applied to offshore wide-angle seismic data: Equatorial and North-West Brazilian Margins. *submitted to Journal of South American Earth Sciences, 31 dec 2022*

Guan, H., Geoffroy, L., Gernigon, L., Chauvet, F., Grigné, C., Werner, P., 2019. Magmatic Ocean-continent transitions. Mar. Pet. Geol. https://doi.org/10.1016/j.marpetgeo. 2019.04.003.

Henry, S. G., Danforth, A., Kumar, N. & Venkatra- man, S. 2009. Paleogeographic mapping of the South Atlantic: Jurassic through Albian evolution. In: AAPG International Conference and Exhibition, 15– 18 November 2009, Rio de Janeiro, Brazil, 645457.pdf.

Jacques, J.M., 2003. A tectonostratigraphic synthesis of the Sub-Andean Basins: implications for the geotectonic segmentation of the Andean Belt. Journal of the Geological Society, London 160, 687–701.

Kashubin, S.N., Petrov, O.V., Artemieva, I.M., Morozov, A.F., Vyatkina, D.V., Golysheva, Yu, S., Kashubina, T.V., Milshtein, E.D., Rybalka, A.V., Erinchek, Yu.M., Sakulina, T.S., krupnova, N.A. and Shulgin, A.A., 2018, Crustal structure of the Mendeleev Rise and the Chukchi Plateau (Artic Ocean) along the Russian wide-angle and multichannel seismic reflection experiement « Artic-2012 ». *Journal of Geodynamics*, 119, 107-122, https://doi.org/10.1016/j.jog.2018.03.006.

Kumar, N., Danforth, A., Nuttal, P., Helwig, J., Bird, D. E. & Venkatraman, S., 2012. From oceanic crust to exhumed mantle: a 40 year (1970-2010) perspective on the nature of crust under the Santos Basin, SE Brazil. , *In*: Mohriak, W.U., Danforth, A., Post, P.J., Brown, D.E., Tari, G.C., Nemcok, M. & Sinha, S.T. (*eds*). Conjugate Divergent Margins. *Geological Society, London, Special Publications*, 369, http://dx.doi.org/10.1144/SP369.16.

Labails, C., Olivet, J.-L., and the Dakhla Study Group, 2009, Crustal structure of the SW Moroccan margin from wide-angle and reflection seismic data (the Dakhla experiment). Part B – The tectonic heritage, *Tectonophysics*, *468*, 83-97.

Lana, M. C., 1985. Rifteamento na bacia de Sergipe-Alagoas, Brasil, Master thesis, 124 pp., Univ. Fed. Ouro Preto, Ouro Preto, Brazil.

Leprêtre, A., Schnürle, P., Evain, M., Verrier, F., Moocroft, D., de Clarens, P., Corela, C., Afilhado, A., Loureiro, A., Leroy, S., d'Acremont, E., Thompson, J., Aslanian, D. and Moulin, M., 2021. Deep structure of the North Natal Valley (Mozambique) using combined wide-angle and reflection seismic data, *JGR, 126*, e2020JB021171. https://doi.org/10.1029/2020JB021171

Leroux, E., Aslanian, D., Rabineau, M., Moulin, M., Granjeon, D., Gorini, C. & Droz, L., 2015. Sedimentary markers: a window to deep geodynamic processes, *Terra Nova*, 27(2), 122-129. http://dx.doi.org/10.1111/ter.12139,

Lister, G.S., Etheridge, M.A., Symonds, P.A., 1986. Detachment faulting and the evolution of passive continental margins. Geology 14, 246–250.

Loureiro, A., Schnürle, P., Klingelhöfer, F., Afilhado, A., Pinheiro, J., Evain, M., Gallais, F., Dias, N., Rabineau, M., Baltzer, A., Benabdellouahed, M., Soares, J., Fuck, R., Cupertino, J. A., Viana, A., Matias, L., Moulin, M., Aslanian, D. & SALSA team. 2018. Imaging exhumed lower continental crust in the distal Jequitinhonha basin, Brazil. *Journal of South American Earth Sciences*, 84, 351-372 http://doi.org/10.1016/j.jsames.2018.01.009.

Loureiro, A. Afilhado, A., Schnürle, P., Evain, M., Dias, N., Klingelhoefer, F., Gallais, F., Pinheiro, J.M., Soares, J., Fuck, R., Cupertino, J.A., Viana, A., Matias, L., Moulin, M., Aslanian, D. & Magic Team, Deep structures of the São Francisco Craton, Camamu and Almada Basins, Brazil. *Submitted to Journal of South American Earth Sciences, 13 Fev 2023*

Ludwig, W. J., Nafe, J. E., Simpson, E. S. W., and Sacks, S., 1968. Seismic-refraction measurements on the Southeast African Continental Margin, J. Geophys. Res., 73, 3707–3719, https://doi.org/10.1029/JB073i012p03707.

Lutter W. J., and R. L. Nowack, 1990. Inversion for crustal structure using reflections of the PASSCAL Ouachita experiment, *Geophysical Journal International*, 95, 4633-4646.

Matos, R.M.D., 1992. The northeast Brazilian rift system. Tectonics 11, 766- 791

McDermott, C., Lonergan, L., Collier, J. S., McDermott, K. G. & Bellingham, P. 2018. Characterization of seaward-dipping reflectors along the South American Atlantic margin and implications for continental breakup. *Tectonics* **37**, 3303–3327.

McKenzie, D., F Nimmo, J. Jackson, P.B., Gans, E.L. Miller, 2000. Characteristics and consequences of flow in the lower crust. *Journal of Geophysical Research*, 105 (B5), 11,029–11,046.

Meyers, J.B., Rosendahl, B.R., Austin, J.A., 1996. Deep penetrating MCS images of the South Basin : implications for rift tectonics and post-breakup salt remobilisation. Basin Research 8, 65–84.

Milani, E. J., and I. Davison, 1988, Basement control and transfer tectonics in the Recôncavo-Tucano-Jatoba rift, Northeast Brazil, *Tectonophysics*, *154*, 41-70.

Mohriak, W.U., Rosendahl, B.R., 2003. Transform zones in the South Atlantic rifted continental margins. Intraplate strike-slip deformation belts: In: Storti, F., Holds- worth, R.E., Salvini, F. (Eds.), Geological Society, London, Special Publication, vol. 210, pp. 211–228.

Mohriak, W. U., 2003. Bacias Sedimentares da Margem Continental Brasiliera., *In: Bizzi, L.A., Schobbenhaus, C., Vidotti, R.M., Gonçalves, J.H. (Eds.), Geologia, Tectônica e Rcursos Mineais do Brasil, Capitulo III. CPRM, Brasilia*, pp. 127–130.

Moulin, M., 2003. Etude géologique et géophysique des marges continentales passives : exemple du Zaïre et de l'Angola. Ph. D Thesis, *Univ de Bretagne Occidentale*, Brest, 2 vol., 360 pp, http://www.ifremer.fr/docelec/doc/2003/these-82.pdf.

Moulin, M., D. Aslanian, J-L. Olivet, I. Contrucci, L. Matias, L. Géli, F. Klingelhoeffer, H. Nouzé, Réhault, J.-P. And Unternehr, P., 2005. Geological constraints on the evolution of the Angolan margin based on reflection and refraction seismic data (ZaïAngo project), *Geophysical Journal International*, *162*, 793-810.

Moulin, M., Aslanian, D., Rabineau, M., Patriat, M. & Matias, L., 2012. Kinematic Keys of the Santos – Namibe Basins, *In*: Mohriak, W.U., Danforth, A., Post, P.J., Brown, D.E., Tari, G.C., Nemcok, M. & Sinha, S.T. (*eds*). Conjugate Divergent Margins. *Geological Society, London, Special Publications*, 369, http://dx.doi.org/10.1144/SP369.3

Moulin, M., Klingelhoefer, F., Afilhado, A., Aslanian, D., Schnürle, P., Nouzé, H., Rabineau, M., Beslier, M.-O. & Feld A., 2015. Deep Crustal Structure Across An Young Passive Margin From Wide- Angle And Reflection Seismic Data (The Sardinia Experiment) – I. Gulf Of Lion's Margin, *Bulletin de la Société Géologique de France*, 186, n°4-5, 309- 330, doi:10.2113/gssgfbull.186.4-5.309

Moulin, M., Aslanian, D., Evain, M., Leprêtre, A., Schnurle, P., Verrier, F., Thompson, J., De Clarens, P., Leroy, S., Dias, N. and PAMELA-MOZ35 Team, 2020. Gondwana breakup: messages from the North Natal Valley, *Terra Nova*. https://doi.org/10.1111/ter.12448

Moulin, M., Schnurle, P., Afilhado, A., Gallais, F., Dias, N., Evain, M., Soares, J., Fuck, R., Neto, O. Viana, A., Aslanian, D. & the MAGIC Team, 2021. Imaging Early Oceanic Crust Spreading in the Equatorial Atlantic Ocean: insights from the MAGIC Wide-Angle Experiment, *Journal of South American Earth Sciences*, 111, https://doi.org/10.1016/j.jsames.2021.103493

Moulin, M., Leprêtre, A., Verrier, F., Schnurle, P., Evain, M., de Clarens, P., Thompson, J., Dias, N., Afilhado, A., Loureiro, A. and D. Aslanian. 2023. From the Lebombo Monocline to the Mozambique Deep Basin, using combined wide-angle and reflection seismic data, *Tectonophysics*, Vol 855. https://doi.org/10.1016/j.tecto.2023.229814.

Oliveira Peixoto, C. L., 2013. Estrutura sísmica da crosta e manto superior dos domínios Maciço Pernambuco-Alagoas, Faixa Sergipana, e porção norte do Cráton do São Francisco: um estudo por refração sísmica profunda, *Master Thesis, Universidade de Brasília Instituto de Geociências, Brasilia*, 48 pp.

Ondréas, H., Aslanian, D., Géli, L., Olivet, J.-L. & Briais, A., 2001. Variations In Axial Morphology, Segmentation And Seafloor Roughness Along The Pacific-Antarctic Ridge Between 56°S And 66°S, Journal of Geophysical Research., Vol. 106, B5, 8521-8546.

Paton, D.A., Pindell, J., McDermott, K., Bellingham, P., Horn, B., 2017. Evolution of seaward-dipping reflectors at the onset of oceanic crust formation at volcanic passive margins: insights from the South Atlantic. Geology 45, 439–442. https:// doi.org/10.1130/G38706.1.

Peron-Pinvidic, G., Manatschal, G., 2008. The final rifting evolution at deep magma-poor passive margins from iberia-newfoundland: a new point of view. Int. J. Earth Sci. 98 (7), 1581–1597. https://doi.org/10.1007/S00531-008-0337-9.

Pinheiro, J.M., Schnurle, P., Evain, M., Afilhado, A., Gallais, F., Klingelhoefer, F., Loureiro, A., Fuck, R., Soares, J., Cupertino, J.A., Viana, A., Rabineau, M., Baltzer, A., Benabdellouahed, M., Dias, N., Moulin, M., Aslanian, D. & SALSA Team, 2018. Lithospheric structuration onshore-offshore of the Sergipe-Alagoas passive margin, NE Brazil, based on wide-angle seismic data. *Journal of South American Earth Sciences*, 88, 649-672, https://doi.org/10.1016/j.jsames.2018.09.015

Rabineau, M, Leroux E., Bache, F., Aslanian, D., Gorini, C., Moulin, M., Molliex, S., Droz, L., Dos Reis, T., Rubino, J.L. & Olivet, J.-L., 2014. Quantifying subsidence and isostatic readjustment using sedimentary paleomarkers, example from the Gulf of Lion, Earth Planetary Science letters, 388, 353-366. http://dx.doi.org/10.1016/j.epsl.2013.11.059 ;

Romito, S. and Mann, P., 2022. Crustal structure of the camamu-almada margin along the northeastern rift segment of brazil from an integration of deep-penetration seismic reflection profiles, refraction, and gravity modeling. *Tectonics*, 41. doi:10.1029/2021tc007157.

Sandwell, D.T., Smith, W.H.F., 1997. Marine gravity anomaly from Geosat and ERS-1 satellite altimetry. J. Geophys. Res. 102, 803–827.

Schneider W.A. & M. Backus, 1964. Ocean-bottom seismic measurements off the California coast, *Journal of Geophysical Research*, 69(6) 1135-1143.

Schnürle, P., Gallais, F., Afilhado, A., Moulin, M., Dias, N., Soares, J., Loureiro, A., Fuck, R., Cupertino, J.A., Viana, A., Aslanian, D. & Magic Team. 2023 Wide-angle Seismic imaging of a transform segment of the Maranhão-Barreirinhas-Ceará margin, NW Brazil. *Journal of South American Earth Sciences.* *https://doi.org/10.1016/j.jsames.2023.104394*.

Schnürle, P., Leprêtre, A., Evain, M., Verrier, F., De-Clarens, P., Dias, N.A., Afilhado, A., Loureiro, A., Leroy, S., d'Acremont, E., Aslanian, D. and Moulin, M. 2023. Crustal structure of the South Mozambique Margin to South Mozambique Ridge from combined wide-angle and reflection seismic data, *Earth and Space Science*, 10. https://doi.org/10.1029/2021EA001902.

Shuck, B.D., VanAvendonk, H., Becel, A, J.A., 2019. The role of mantle melts in the transition from rifting to seafloor spreading offshore eastern North America. Earth Planet Sci. Lett. 525, 115756 https://doi.org/10.1016/j.epsl.2019.115756.

Shulgin, A., Mjelde, R., Faleide, J. I., Hoy, T., Flueh, E., & Thybo, H., 2018. The crustal structure in the transition zone between the western and eastern Barents Sea. *Geophysical Journal International*, *214*, 315–330. https://doi.org/10.1093/gji/ggy139

Sibuet, J.-C., Tucholke, B., 2012. The geodynamic province of transitional lithosphere adjacent to magma-poor continental margins. In: Mohriak, W.U., Danforth, A., Post, P.J., Brown, D.E., Tari, G.C., Nemcok, M., Sinha, S.T. (Eds.), Conjugate Divergent Margins. Geological Society, London, Special Publications, vol. 369. https://doi.org/10.1144/SP369.15.

Soares J.E.P., Berrocal J., Fuck R.A., Mooney W.D. & Ventura D.B.R., 2006. Seismic characteristics of the central Brazil crust and upper mantle: A deep seismic refraction study, *Journal of Geophysical Research*, *111*, B12302, doi:12310.11029/12005JB003769.

Soares, J. E. P., de Lima, M. V., Fuck, R. A., & Berrocal, J., 2010. Características sísmicas da litosfera da Província Borborema : resultados parciais do experimento de refração sísmica profunda, *IV Simpósio Brasileiro da SBGf – Brasília 2010.*

Tavares, E. J., Soares, J. E. P., Fuck, R. A., & De Lima, M. V. A., 2012. Modelagem de onda P e razão Vp/Vs da crosta sob a linha de refração sísmica profunda NW-SE da Província Borborema, *V Simpósio Brasileiro da SBGf – Brasília 2012*.

Thinon, I., Matias, L., Réhault, J. P., Hirn, A., Fidalgo-Gonzalez, L. & Avedik, F., 2003. Deep structure of the Armorican Basin (Bay of Biscay): a review of Norgasis seismic reflection and refraction data. *Journal of the Geological Society, London*, 160, 99-116. doi:10.1144/0016-764901-103

Thybo, H., Nielsen, C.A., 2009. Magma-Compensated Crustal Thinning In Continental Rift Zones. Nature 457, 873-876.

Tozer, B., Watts, A.B., Daly, M.C., 2017. Crustal structure, gravity anomalies, and subsidence history of the Parnaíba cratonic basin, Northeast Brazil. J. Geophys. Res.: Solid Earth 122, 5591–5621. https://doi.org/10.1002/2017J B014348.

Ussami, N., Karner, G.D., Bott, M.H.P., 1986. Crustal detachment during South Atlantic rifting and formation of Tucano-Gabon basin system, *Nature*, *332*, 629-632.

Vlastelic, I., Dosso, L., Bougault, H., As- lanian, D., Géli, L., Etoubleau, J., Bohn, M., Joron, J. L. And Bollinger, C., 2000. Chemical Systematics Of An Intermediate Spreading Ridge: The Pacific-Antarctic Ridge Between 56 And 66°S, *J. Geophys. Res.*, 105, 2915-2936.

Wernicke, B., 1985. Uniform-Sense Normal Simple Shear Of The Continental Lithosphere. Can. *Journal Of Earth Sci.* 22, 22.108-22.125.

White, R. S., McKenzie, D., & O'Nions, R. K., 1992. Oceanic crustal thickness from seismic measurements and rare earth element inversions. *Journal of Geophysical Research*, *97*, 19683–19715. https://doi. org/10.1029/92JB01749.

Zelt C.A. & R.B. Smith, 1992. Seismic travel time inversion for 2-D crustal velocity structure, *Geophysical Journal International*, 108, 16-34.

phase	npts	Trms	chi-squared
Pw	2703	0.029	0.414
Ps2P	215	0.031	0.390
Ps2	209	0.025	0.246
Ps3P	329	0.022	0.186
Ps3	16	0.042	0.751
Ps4P	26	0.054	1.192
Ps4	214	0.021	0.177
Ps5P	287	0.037	0.547
Ps5	65	0.030	0.376
Ps6P	112	0.029	0.347
Ps6	289	0.047	0.887
Ps7P	293	0.031	0.398
Ps7	127	0.028	0.316
Ps8P	381	0.017	0.118
Ps8	182	0.023	0.217
PuP	201	0.028	0.318
Pu	372	0.044	0.777
Pg1P	145	0.046	0.852
Pg1	818	0.194	0.868
Pg2P	8	0.055	0.088
Pg2	1838	0.165	2.486
Pg3P	225	0.166	1.175
Pg3	2601	0.055	1.205
PbmP	923	0.056	1.276
Pbm	2150	0.261	2.786
PmP	878	0.412	5.841
Pn1	2055	0.161	1.828
Pn2P	495	0.352	1.382
Pn2	6841	0.251	1.009

Instruments	shot	dir	npts	Trms	chi-squared
SL07BLAST01	-254.348	-1	3	0.176	0.745
	-254.348	1	41	0.260	1.108
SL07BLAST02	-253.317	-1	3	0.205	1.010
	-253.317	1	46	0.247	0.996
SL07BLAST03	-255.071	-1	3	0.198	0.938
	-255.071	1	49	0.351	2.016
SL07LSS01	-269.139	1	223	0.230	0.853
SL07LSS02	-264.808	1	26	0.332	1.831
SL07LSS03	-258.780	1	117	0.205	0.677
SL07LSS04	-254.550	1	294	0.183	0.540
SL07LSS05	-249.442	1	433	0.180	0.520
SL07LSS06	-244.627	1	396	0.166	0.442
SL07LSS07	-238.818	1	283	0.359	2.065
SL07LSS08	-235.118	1	541	0.140	0.312
SL07LSS09	-229.513	1	423	0.172	0.474
SL07LSS10	-224.447	1	425	0.115	0.213
SL07LSS11	-219.422	1	375	0.207	0.689
SL07LSS12	-214.568	1	336	0.409	2.683
SL07LSS13	-209.130	X	X	X	X
SL07LSS14	-203.916	X	X	X	X
SL07LSS15	-199.163	1	73	0.363	2.505
SL07LSS16	-193.520	1	146	0.302	1.471
SL07LSS17	-188.402	1	320	0.206	0.681
SL07LSS18	-184.218	1	597	0.420	3.180
SL07LSS19	-178.856	1	202	0.404	3.789
SL07LSS20	-174.351	1	9	0.232	0.967
SL07LSS21	-169.239	1	104	0.299	1.893
SL07LSS22	-164.149	1	196	0.179	0.632
SL07LSS23	-159.497	1	343	0.335	2.252
SL07LSS24	-154.175	1	196	0.332	2.289
SL07LSS25	-149.243	1	358	0.338	1.940
SL07LSS26	-144.199	1	182	0.304	1.752
SL07LSS27	-139.250	1	21	0.345	3.133
SL07LSS28	-134.362	1	346	0.255	1.252
SL07LSS29	-129.326	X	X	X	X
SL07LSS30	-124.447	1	64	0.457	2.891
SL07LSS31	-119.419	1	302	0.259	1.365
SL07LSS32	-113.848	1	725	0.118	0.290
SL07LSS33	-109.305	1	136	0.279	1.020
SL07LSS34	-104.460	1	515	0.123	0.325
SL07LSS35	-99.289	1	754	0.168	0.537
SL07LSS36	-93.986	1	830	0.247	1.001
SL07LSS37	-89.336	1	986	0.231	0.805
SL07LSS38	-84.455	1	124	0.168	0.485
SL07LSS39	-79.108	1	979	0.142	0.388
SL07LSS40	-74.370	1	684	0.286	1.963

SL07LSS41	-69.295	1	426	0.184	0.501
SL07LSS42	-64.404	1	682	0.235	1.208
SL07LSS43	-59.476	1	683	0.208	0.798
SL07LSS44	-54.413	X	X	X	X
SL07LSS45	-49.399	1	37	0.134	0.459
SL07LSS46	-44.337	1	707	0.121	0.367
SL07OBS01	0.000	-1	61	0.035	0.510
	0.000	1	497	0.163	10.663
SL07OBS02	12.440	-1	225	0.062	1.569
	12.440	1	657	0.086	2.964
SL07OBS03	25.009	-1	336	0.082	2.696
	25.009	1	484	0.043	0.729
SL07OBS04	37.390	-1	334	0.065	1.689
	37.390	1	689	0.050	1.013
SL07OBS05	49.885	-1	489	0.094	3.539
	49.885	1	619	0.068	1.851
SL07OBS06	62.218	-1	523	0.056	1.274
	62.218	1	558	0.032	0.408
SL07OBS07	74.515	-1	732	0.040	0.628
	74.515	1	669	0.026	0.262
SL07OBS09	99.279	-1	708	0.038	0.666
	99.279	1	622	0.026	0.486
SL07OBS10	111.828	-1	829	0.032	0.402
	111.828	1	507	0.023	0.218
SL07OBS11	124.076	-1	817	0.044	0.784
	124.076	1	420	0.023	0.205
SL07OBS12	136.787	-1	706	0.047	0.901
	136.787	1	196	0.020	0.157

phase	npts	Trms	chi-squared
Pw	2334	0.025	0.691
Ps1	0	X	X
Ps2P	241	0.036	0.517
Ps2	290	0.032	0.408
Ps3P	386	0.030	0.364
Ps3	141	0.022	0.199
Ps4P	401	0.034	0.470
Ps4	101	0.025	0.253
Ps5P	287	0.027	0.294
Ps5	185	0.022	0.192
Ps6P	118	0.021	0.175
Ps6	288	0.020	0.167
Ps7P	642	0.027	0.286
Ps7	483	0.029	0.341
Pg1P	326	0.046	0.846
Pg1	749	0.053	1.111
Pg2P	116	0.034	0.455
Pg2	2754	0.042	0.722
PuP	375	0.052	0.431
Pu	1130	0.050	0.988
Pm1P	954	0.074	0.863
Pn	1384	0.074	0.849
Pm2P	155	0.079	0.635

Instrument	shot	dir	npts	Trms	chi-squared
SL08OBS01	149.338	-1	480	0.044	0.562
	149.338	1	428	0.030	0.451
SL08OBS02	136.911	-1	528	0.028	0.265
	136.911	1	458	0.030	0.358
SL08OBS03	124.474	-1	539	0.029	0.313
	124.474	1	476	0.036	0.402
SL08OBS04	111.968	-1	601	0.052	1.154
	111.968	1	611	0.040	0.434
SL08OBS05	99.583	-1	587	0.046	0.616
	99.583	1	699	0.046	0.502
SL08OBS06	87.219	-1	664	0.042	0.630
	87.219	1	753	0.036	0.435
SL08OBS07	74.815	-1	634	0.045	0.559
	74.815	1	776	0.058	0.826
SL08OBS08	62.457	-1	695	0.048	0.494
	62.457	1	648	0.049	0.531
SL08OBS09	49.948	-1	598	0.042	0.692
	49.948	1	719	0.043	0.347
SL08OBS10	37.541	-1	273	0.035	0.507
	37.541	1	45	0.039	0.447
SL08OBS11	24.920	-1	172	0.076	3.800
	24.920	1	502	0.074	2.138
SL08OBS12	12.694	-1	155	0.034	0.877
	12.694	1	756	0.071	1.254
SL08OBS13	0.000	-1	24	0.029	0.354
	0.000	1	419	0.032	0.412

FIGURE 1

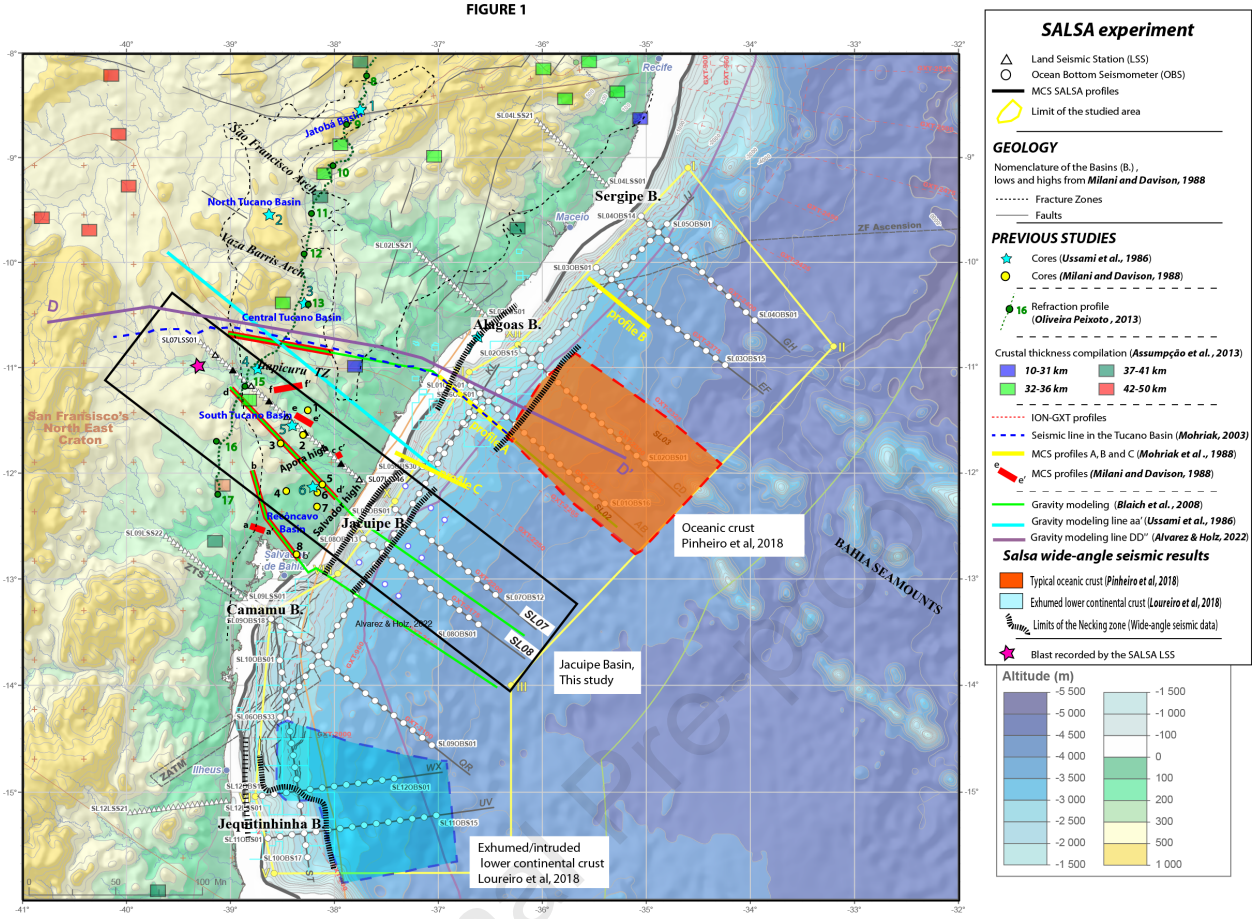

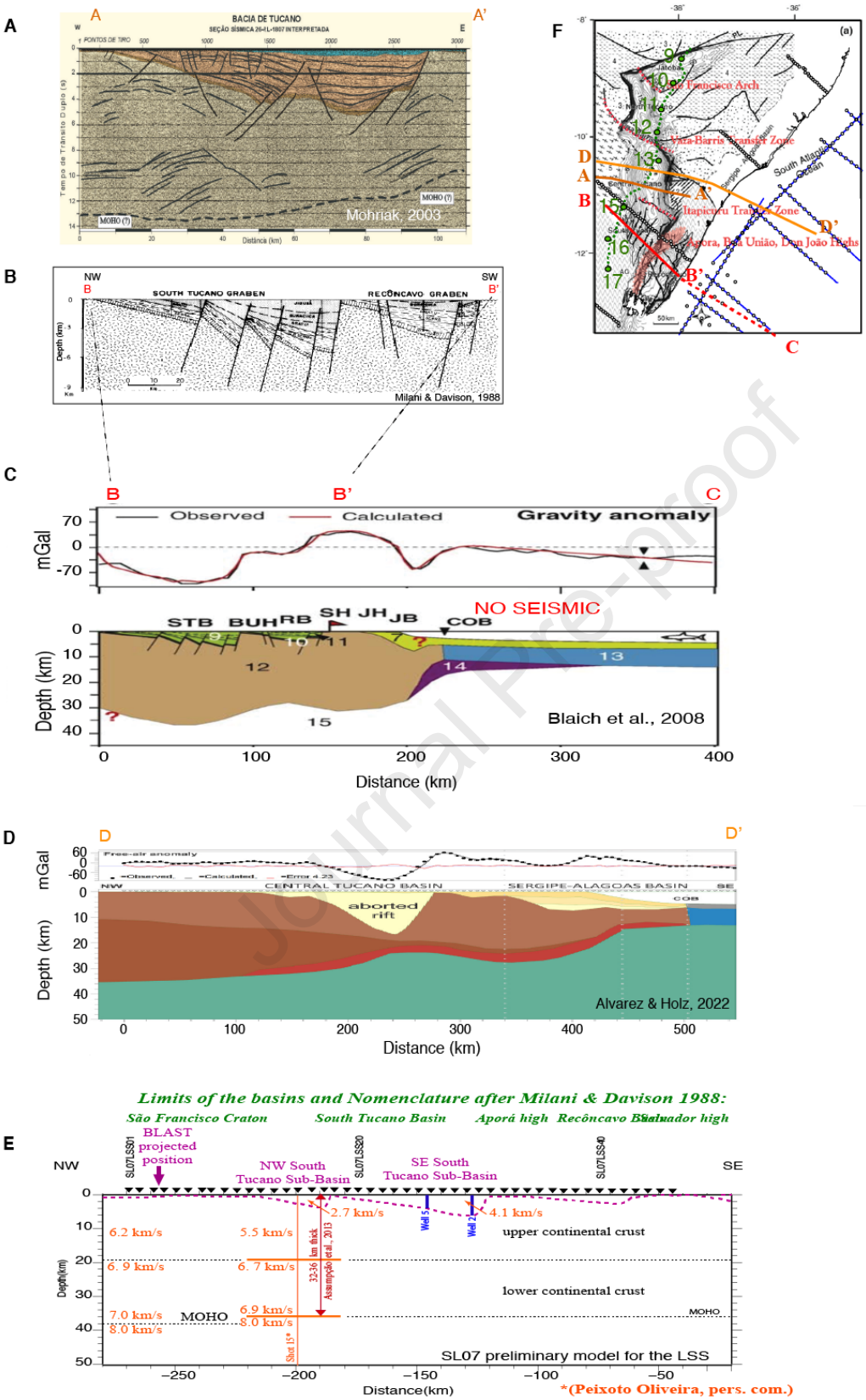
A
A'
BACIA DE TUCANO
SEÇÃO SÍSMICA 26-FL-1807 INTERPRETADA
Mohriak, 2003
B
NW
SW
SOUTH TUCANO GRABEN
RECÔNCAVO GRABEN
Milani & Davison, 1988
C
B
B'
C
Observed
Calculated
Gravity anomaly
mGal
NO SEISMIC
STB
BUH
RB
SH
JH
JB
COB
Depth (km)
Blaich et al., 2008
Distance (km)
D
D'
Free-air anomaly
CENTRAL TUCANO BASIN
SERGIPE-ALAGOAS BASIN
aborted rift
Alvarez & Holz, 2022
Limits of the basins and Nomenclature after Milani & Davison 1988:
São Francisco Craton
South Tucano Basin
Aporá high
Recôncavo Basin
Salvador high
E
NW
SE
BLAST projected position
NW South Tucano Sub-Basin
SE South Tucano Sub-Basin
6.2 km/s
5.5 km/s
2.7 km/s
4.1 km/s
upper continental crust
6.9 km/s
6.7 km/s
lower continental crust
7.0 km/s
8.0 km/s
MOHO
6.9 km/s
8.0 km/s
SL07 preliminary model for the LSS
Distance(km)
*(Peixoto Oliveira, pers. com.)
F
(a)
Jacobina
Salvador Curaçaca Arch
Vaza-Barris Transfer Zone
South Atlantic Ocean
Itapicuru Transfer Zone
Sergipe, Boa União, Dom João Heights
50km

FIGURE 2

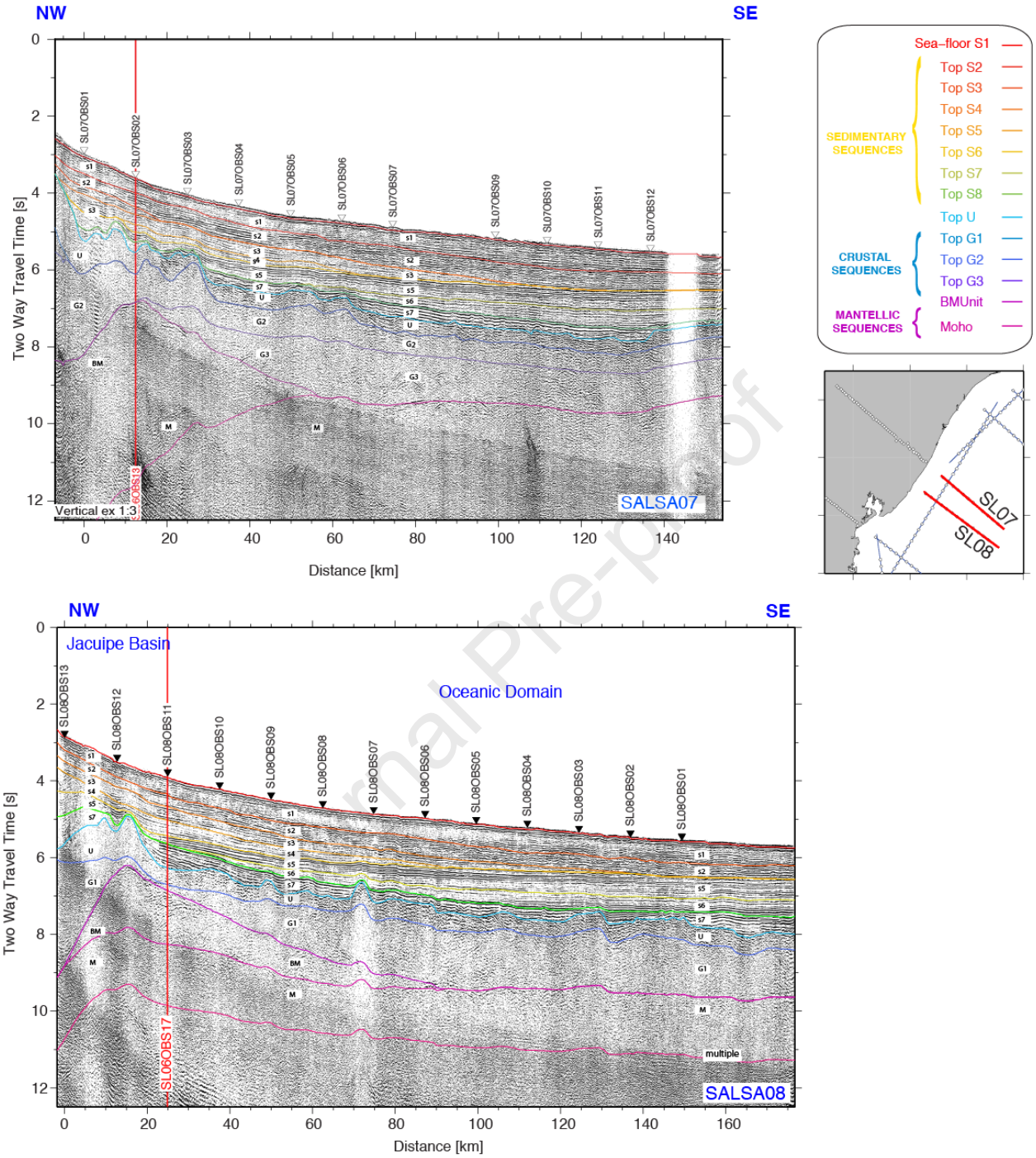
NW
SE
Two Way Travel Time [s]
Distance [km]
SL07OBS01
SL07OBS02
SL07OBS03
SL07OBS04
SL07OBS05
SL07OBS06
SL07OBS07
SL07OBS09
SL07OBS10
SL07OBS11
SL07OBS12
SL06OBS13
Vertical ex 1.3
SALSA07
Sea–floor S1
Top S2
Top S3
Top S4
Top S5
Top S6
Top S7
Top S8
Top U
Top G1
Top G2
Top G3
BMUnit
Moho
SEDIMENTARY SEQUENCES
CRUSTAL SEQUENCES
MANTELLIC SEQUENCES
SL07
SL08
NW
SE
Jacuipe Basin
Oceanic Domain
Two Way Travel Time [s]
Distance [km]
SL08OBS13
SL08OBS12
SL08OBS11
SL08OBS10
SL08OBS09
SL08OBS08
SL08OBS07
SL08OBS06
SL08OBS05
SL08OBS04
SL08OBS03
SL08OBS02
SL08OBS01
SL06OBS17
multiple
SALSA08

FIGURE 5

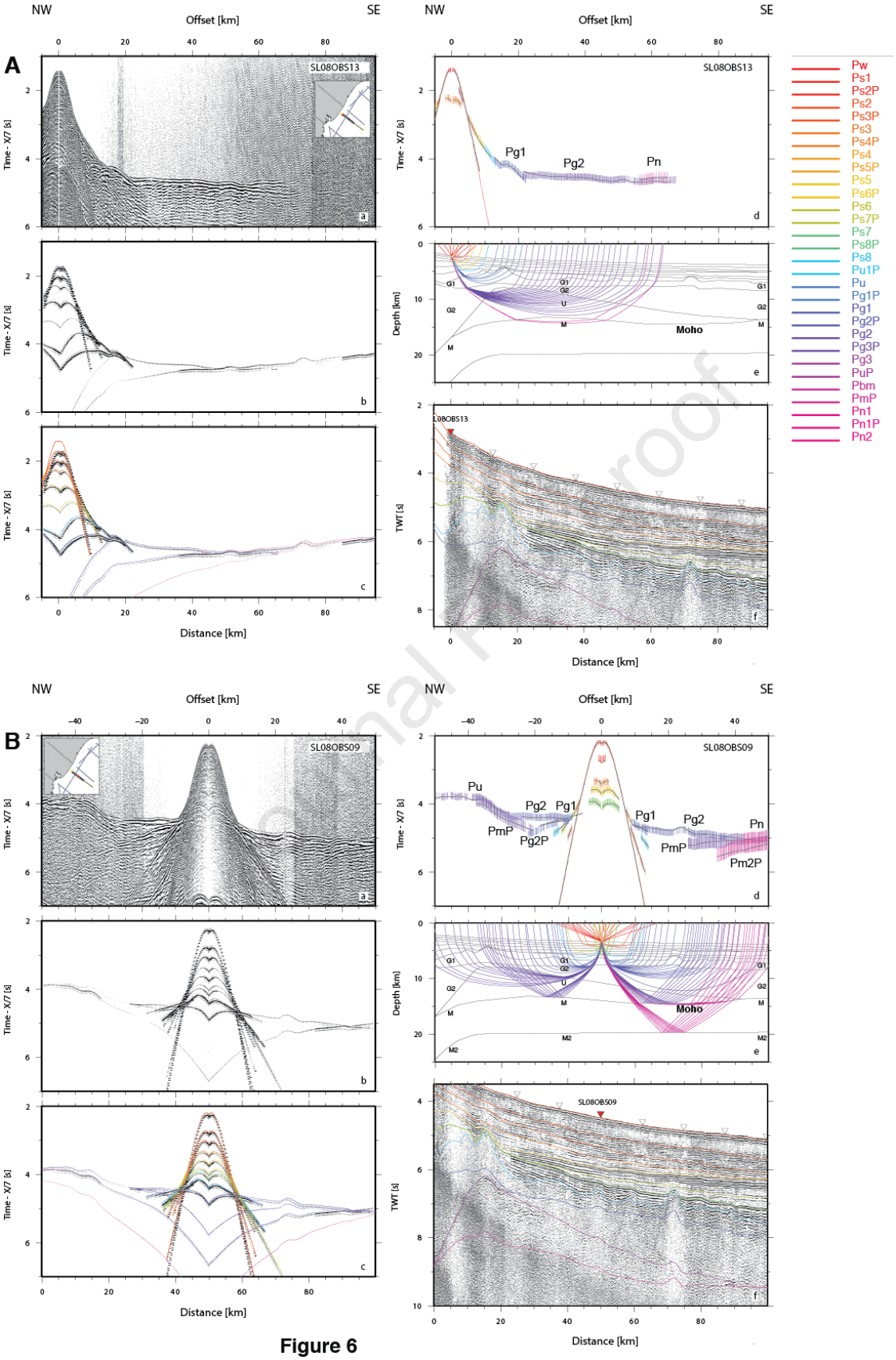
A
NW
SE
Offset [km]
SL08OBS13
Time - X/7 [s]
Pg1
Pg2
Pn
Depth [km]
G1
G2
U
M
Moho
TWT [s]
Distance [km]
B
SL08OBS09
Pu
PmP
Pg2P
Pm2P
M2
Pw
Ps1
Ps2P
Ps2
Ps3P
Ps3
Ps4P
Ps4
Ps5P
Ps5
Ps6P
Ps6
Ps7P
Ps7
Ps8P
Ps8
Pu1P
Pu
Pg1P
Pg1
Pg2P
Pg2
Pg3P
Pg3
PuP
Pbm
PmP
Pn1
Pn1P
Pn2

Figure 6

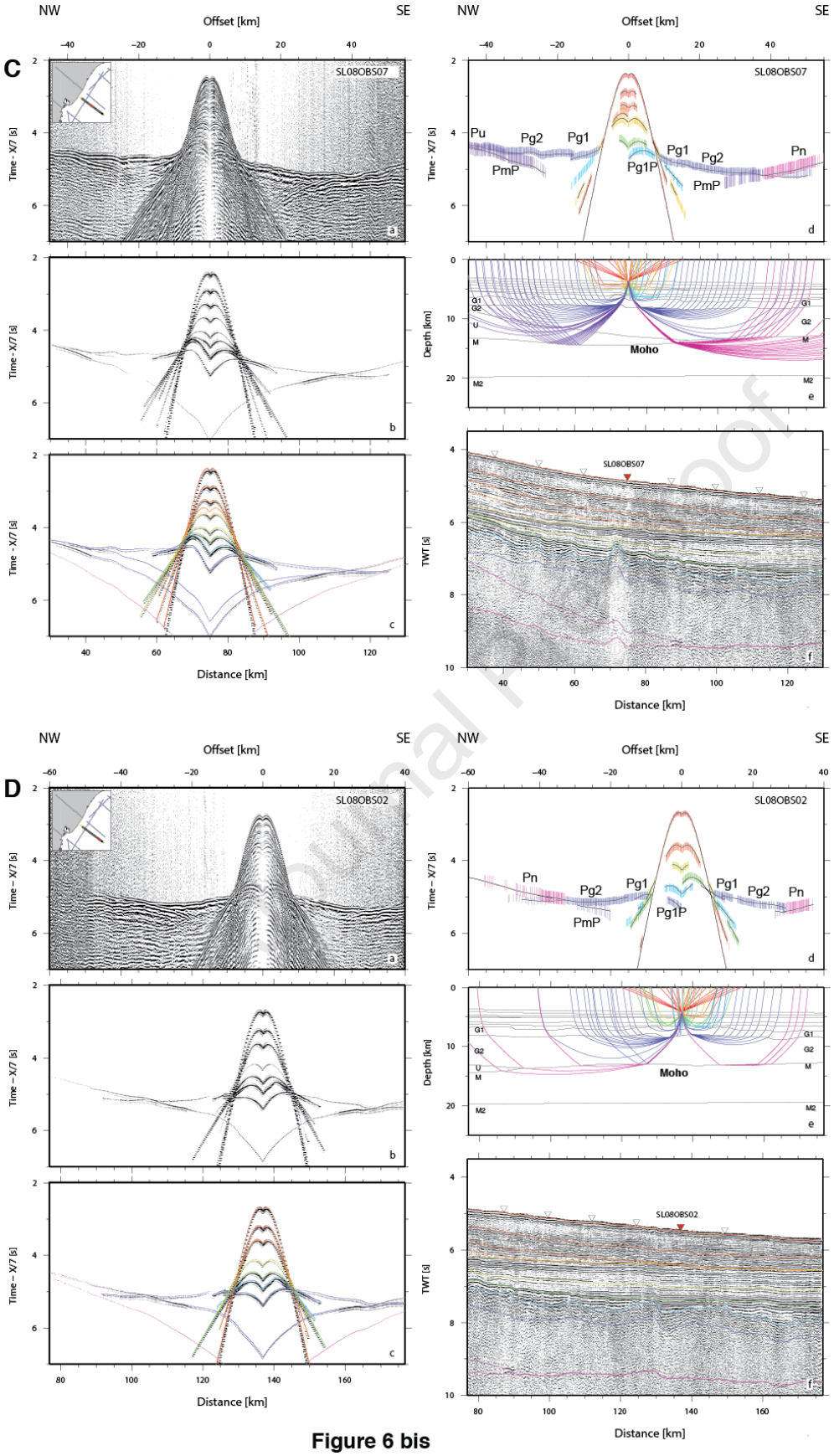
C
NW
SE
Offset [km]
SL08OBS07
Time - X/7 [s]
Pu
Pg2
Pg1
PmP
Pg1P
Pn
Depth [km]
Moho
TWT [s]
Distance [km]
D
SL08OBS02

Figure 6 bis

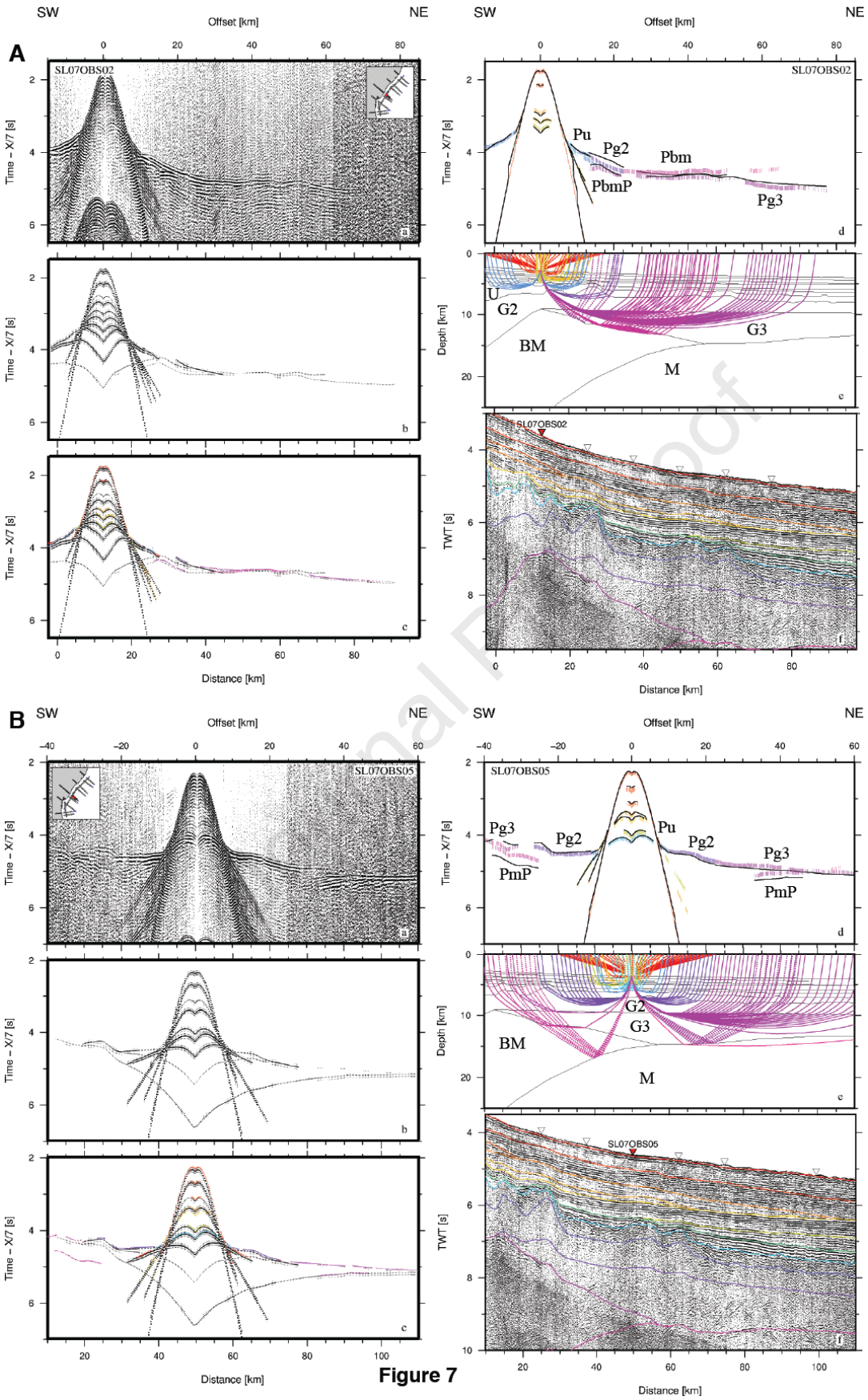
A
SW
NE
Offset [km]
SL07OBS02
Time – X/7 [s]
Pu
Pg2
Pbm
PbmP
Pg3
Depth [km]
U
G2
G3
BM
M
TWT [s]
Distance [km]
B
SL07OBS05
PmP

Figure 7

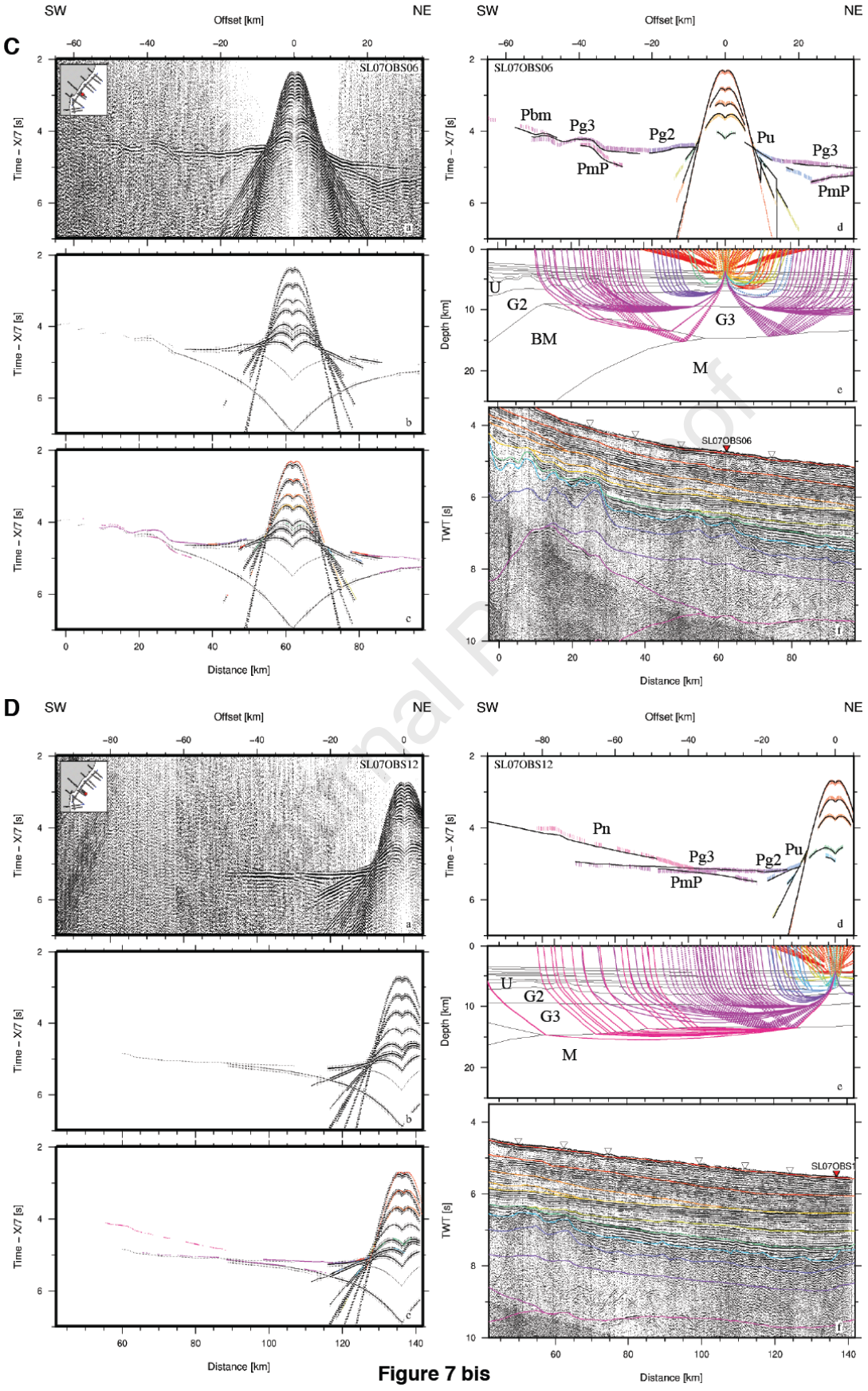
C
SW
NE
Offset [km]
SL07OBS06
Pbm
Pg3
Pg2
Pu
PmP
U
G2
G3
BM
M
Time – X/7 [s]
Depth [km]
TWT [s]
Distance [km]
D
SL07OBS12
Pn
SL07OBS1

Figure 7 bis

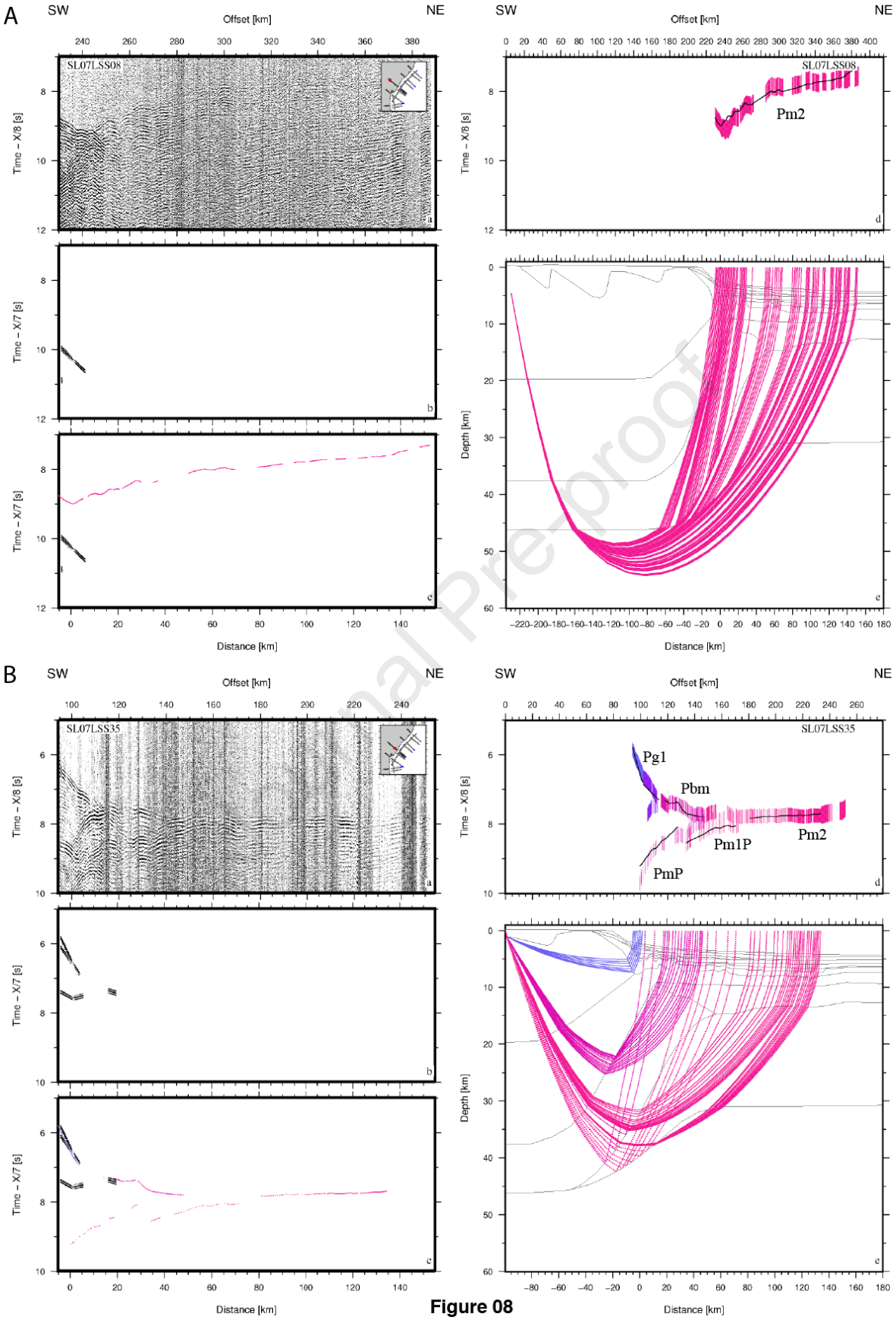
A
SW
NE
Offset [km]
SL07LSS08
Time – X/8 [s]
Time – X/7 [s]
Distance [km]
Depth [km]
Pm2
B
SL07LSS35
Pg1
Pbm
Pm1P
PmP

Figure 08

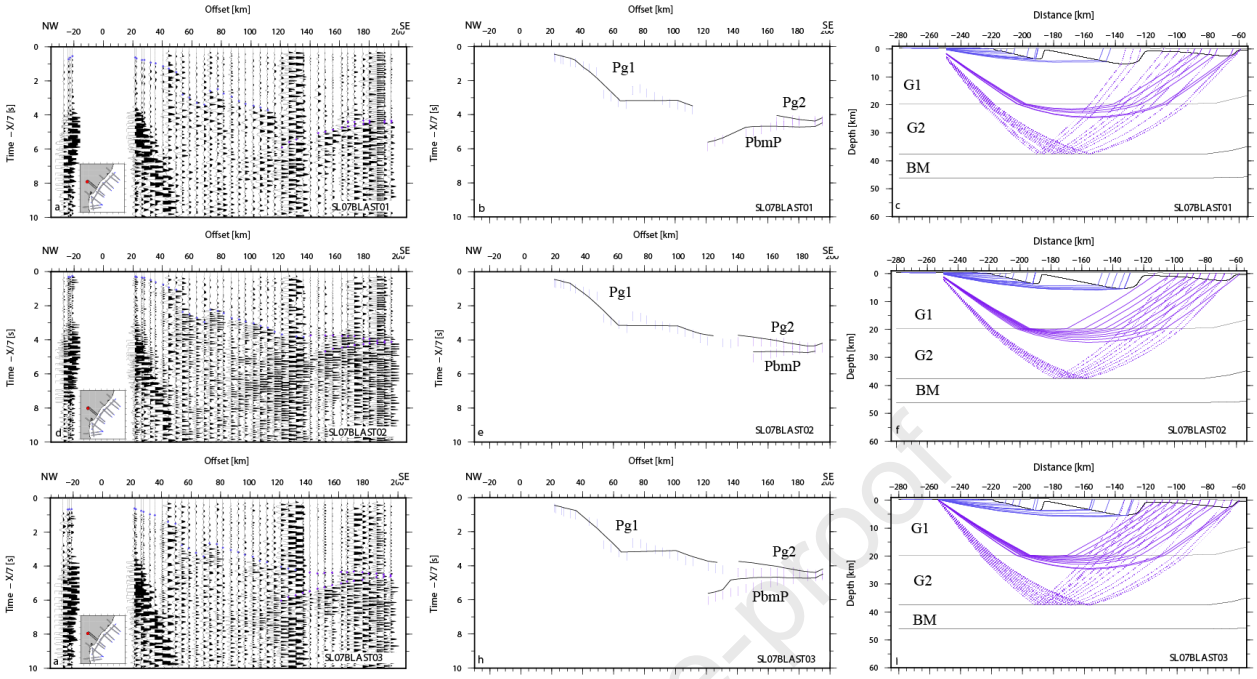

Figure 09

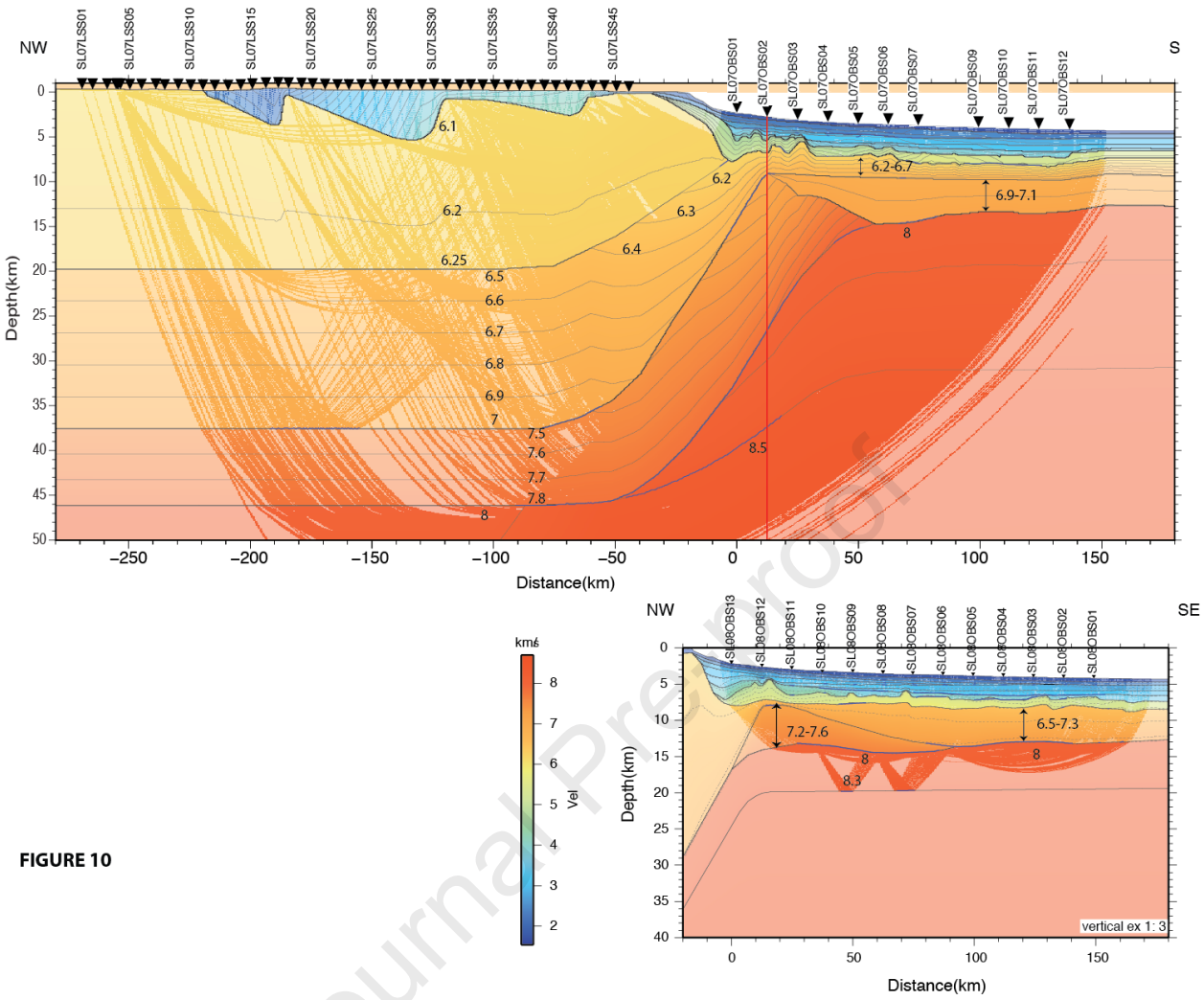

FIGURE 10

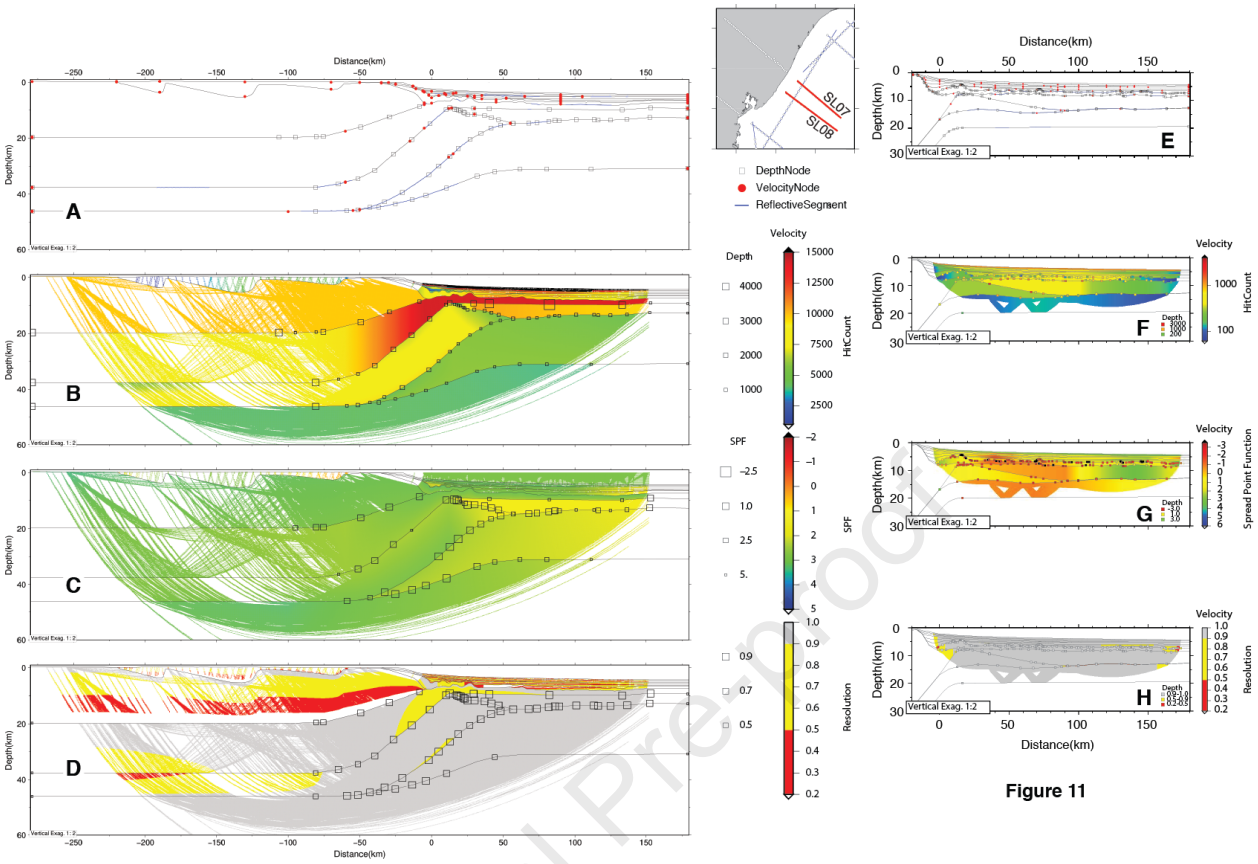

Figure 11

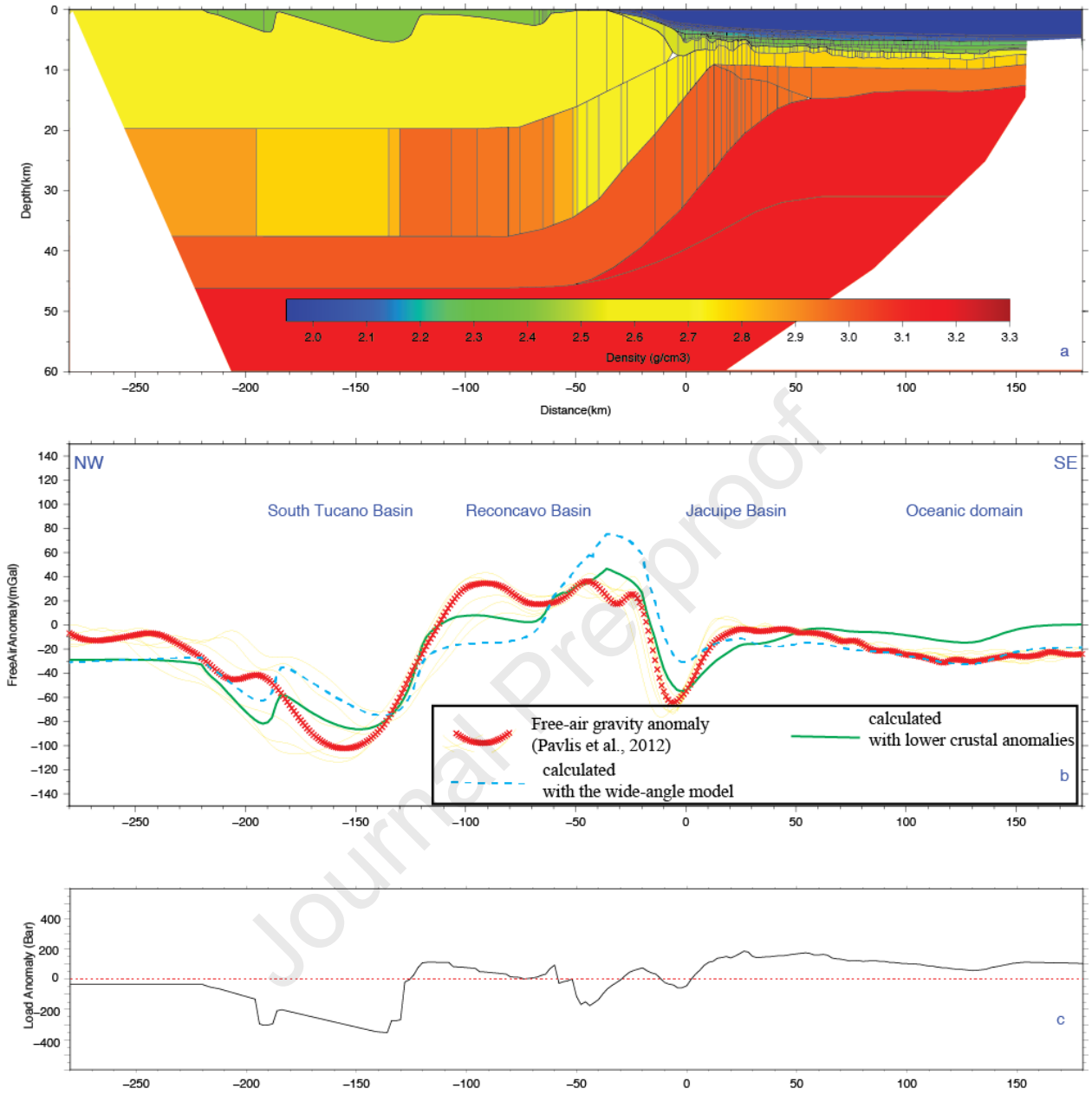

FIGURE 12

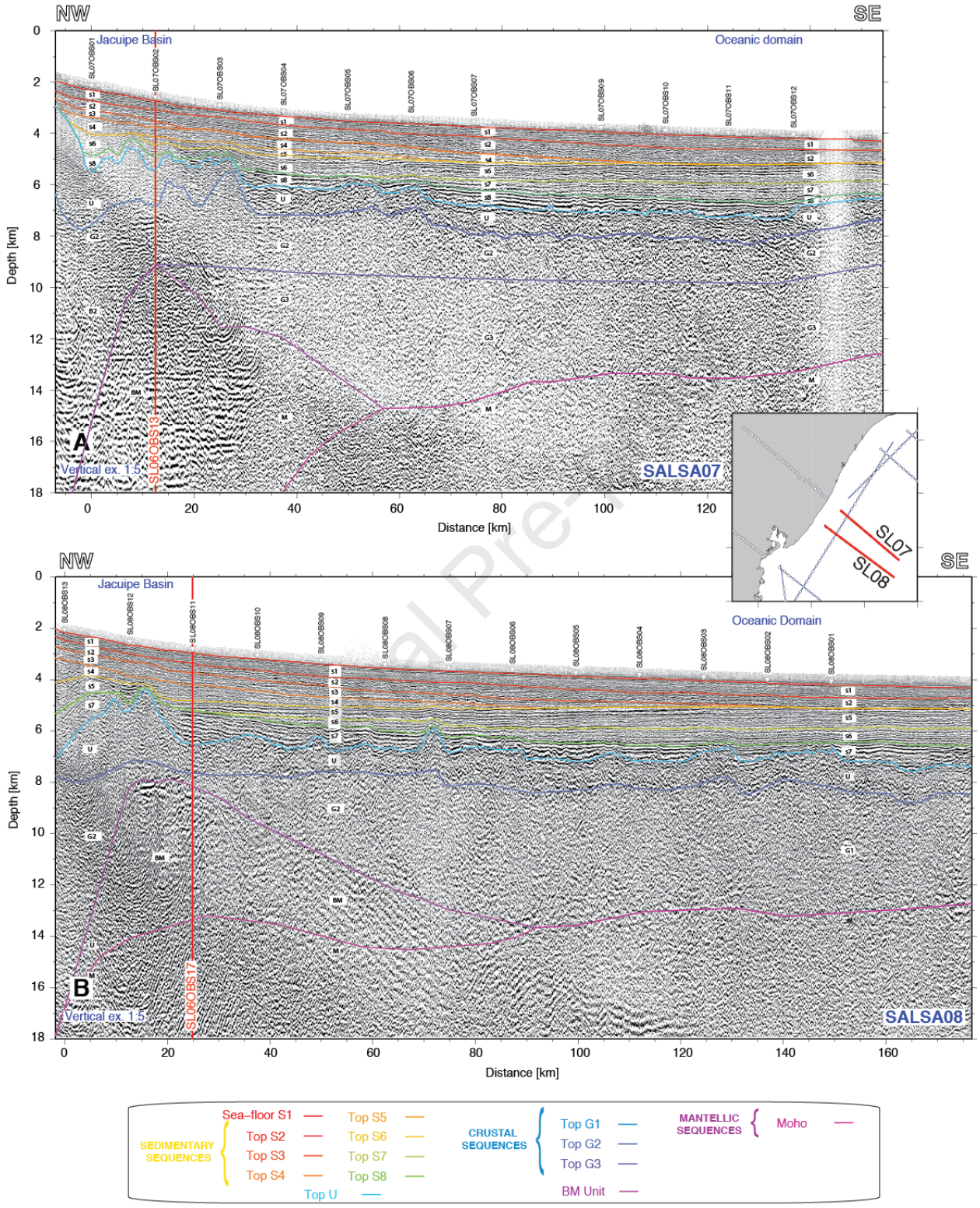
NW
SE
Jacuipe Basin
Oceanic domain
A
Vertical ex. 1:5
SL06OBS13
SALSA07
Depth [km]
Distance [km]
SL07
SL08
Oceanic Domain
B
Vertical ex. 1:5
SL06OBS17
SALSA08
SEDIMENTARY SEQUENCES
Sea-floor S1
Top S2
Top S3
Top S4
Top S5
Top S6
Top S7
Top S8
Top U
CRUSTAL SEQUENCES
Top G1
Top G2
Top G3
BM Unit
MANTELLIC SEQUENCES
Moho

Figure 13

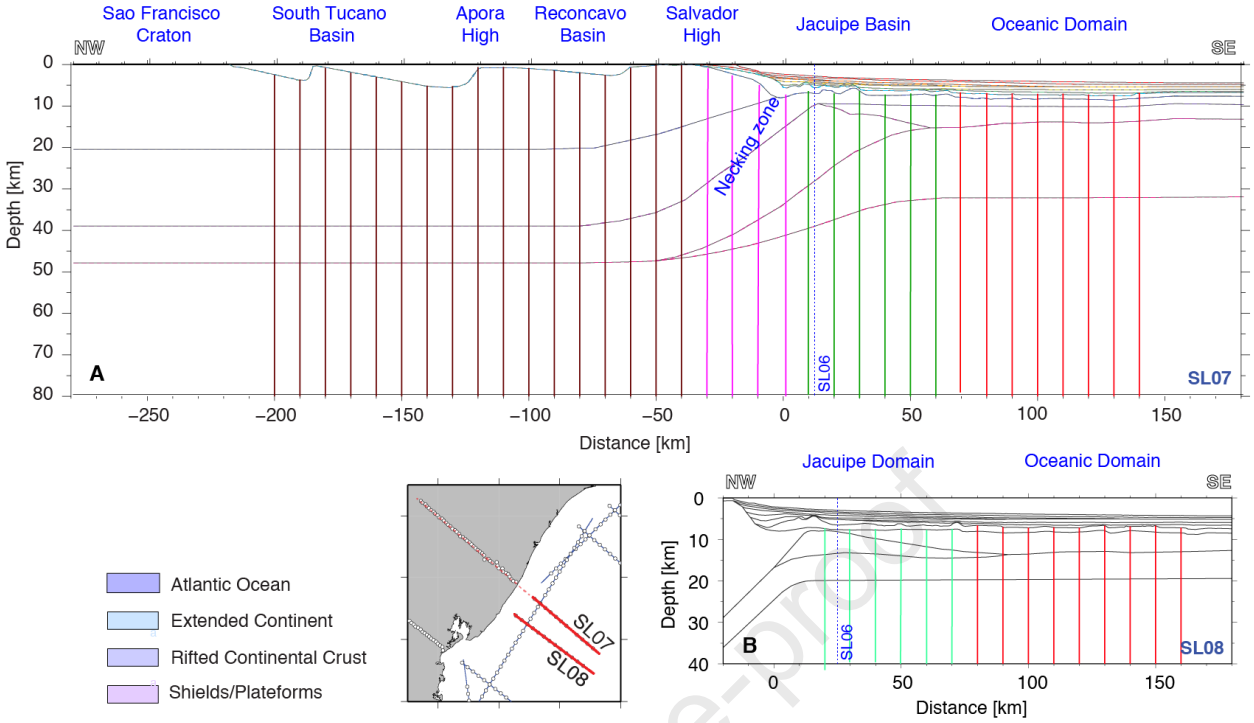

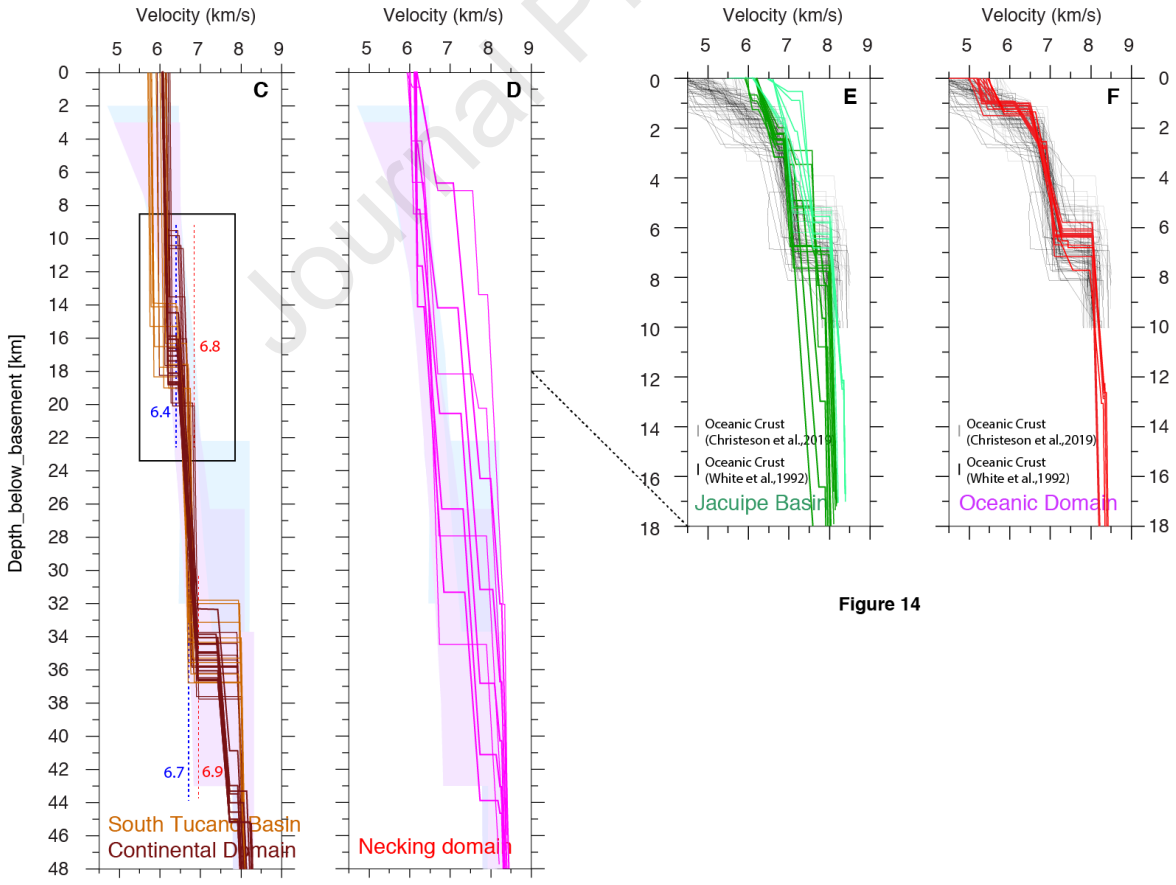

Figure 14

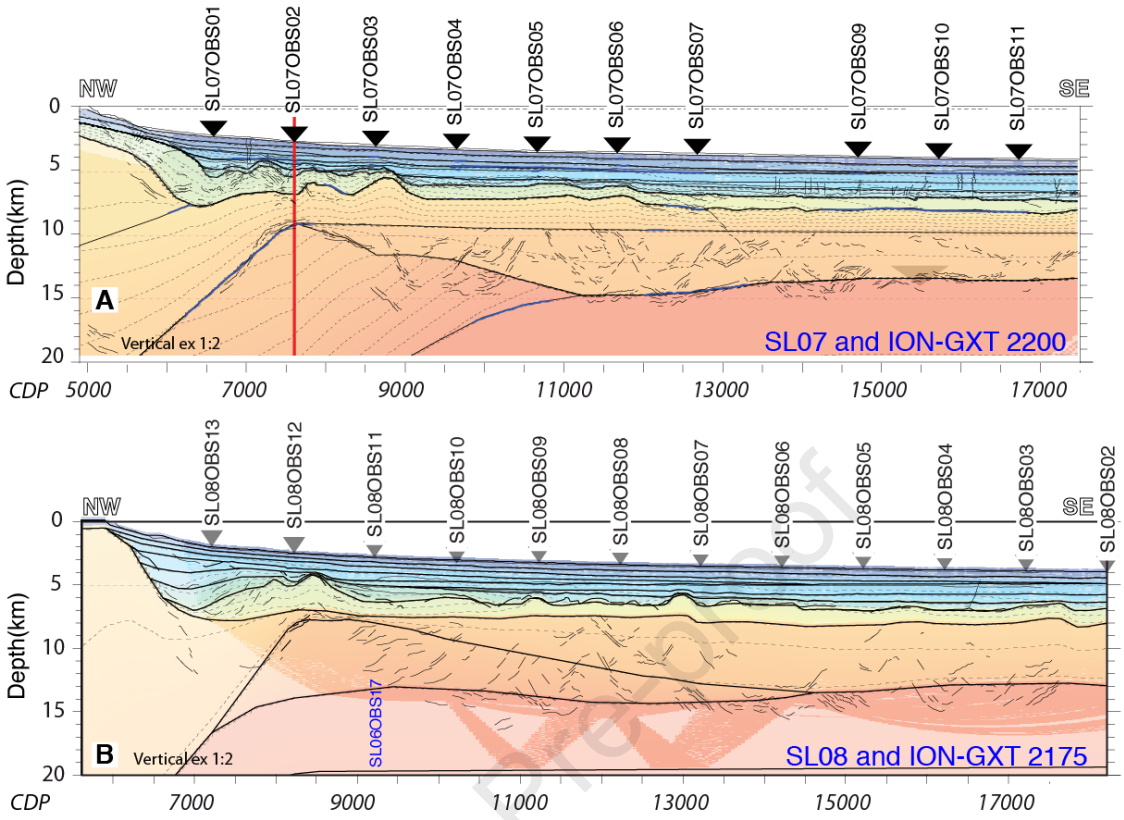

Figure 15

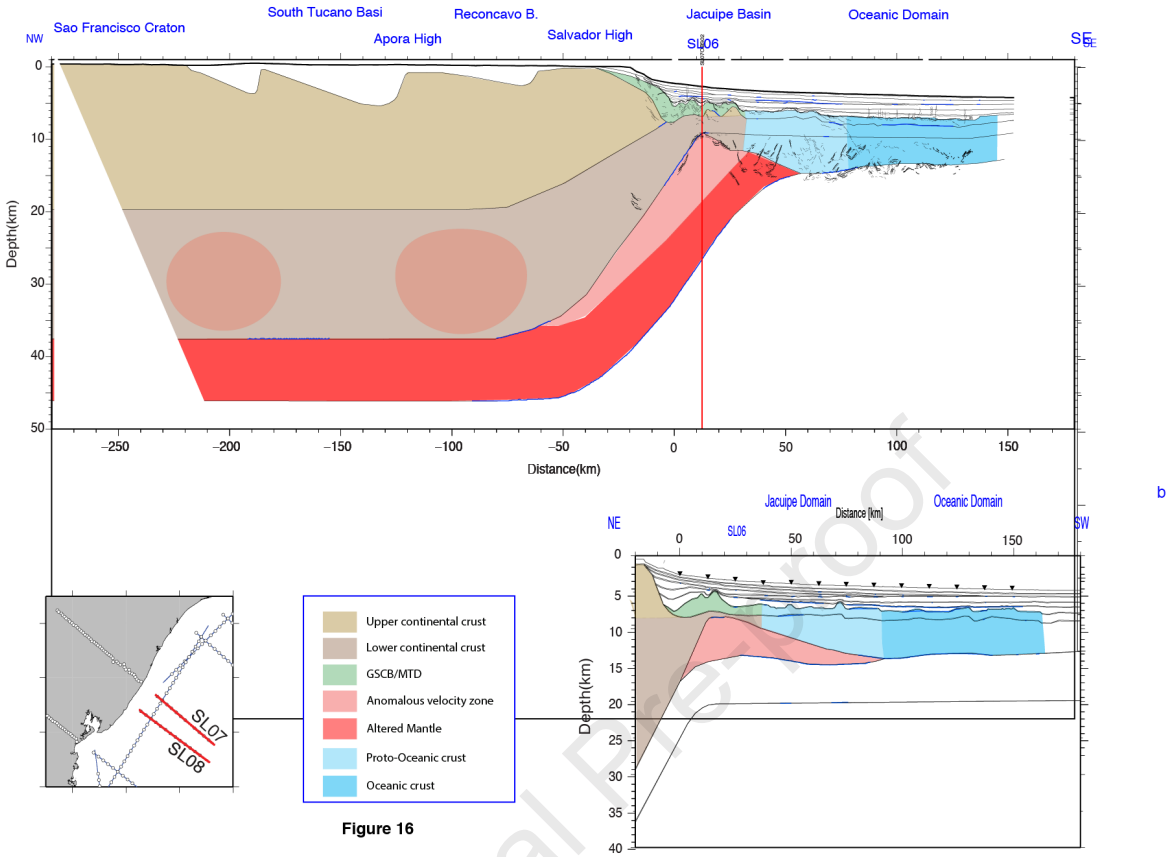

Figure 16

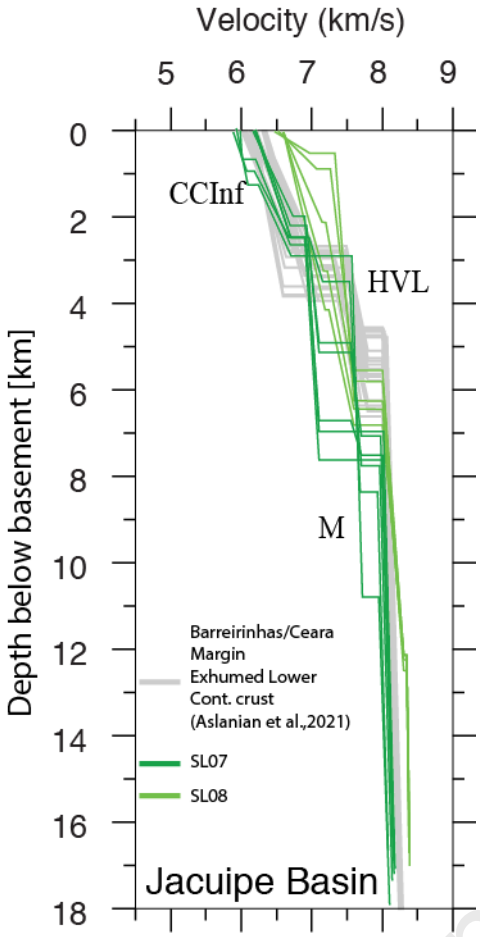

FIGURE 17

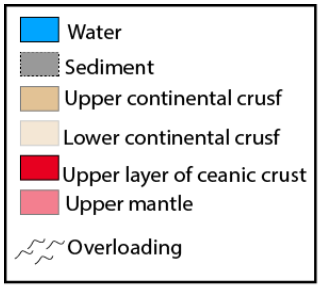

FIGURE 18

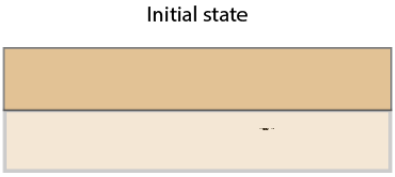

A] Overloading of the lower crust: Intrusion? Phase transformation?
(Parnaiba: Tozer et al., 2017 - Baikal: Thybo & Nielsen, 2009 - Tucano: Aslanian et al., this issue)

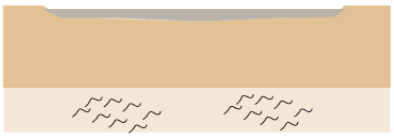

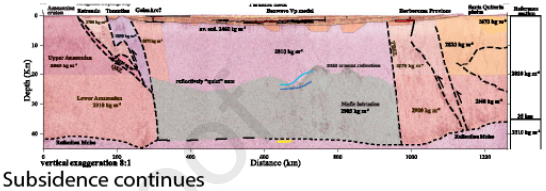

B] Overloading of the lower crust: Vertical Subsidence continues
(Natal Valley: Lepretre et al, 2021; Moulin et al, 2020; Schnurle et al., in press
- Angola: Moulin et al., 2005; Aslanian et al., 2009; Mendeleev ridge: Kashubin et al., 2018)

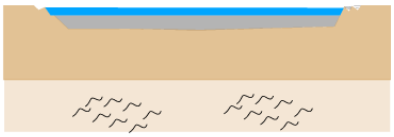

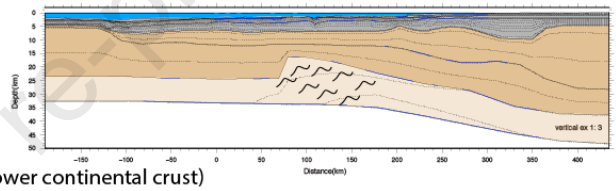

C] Exhumation Phase (lower continental crust)
(Africa/Brazilian Margins, Aslanian et al, 2009, 2012; Evain et al., 2015 ; Loureiro et al., 2018
Provençal Basin: Moulin et al., 2015, Afilhado et al., 2015; Jolivet et al., 2015; Becel et al., 2020; Guan et al., 2019; Chauvet et al., 2021)

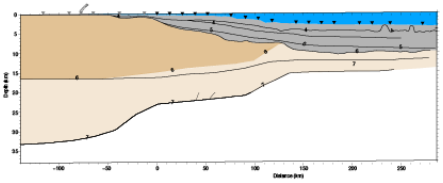

D] Proto-oceanic crust (lower continental crust + Intrusion) and subsidence increase
(North Brazilian margin: Aslanian et al., 2021; Moulin et al., 2021
Angola Margin: Moulin et al., 2005; Aslanian et al., 2009; Santos Basin, Evain et al., 2015
Provençal Basin: Moulin et al. 2015; Afilhado et al, 2015)

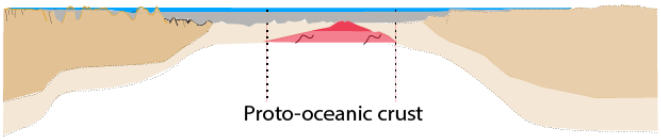

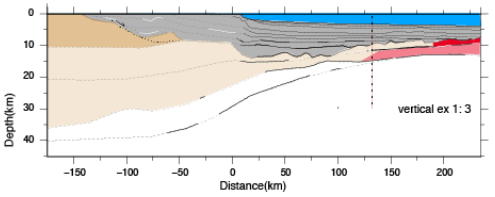

A) Hypothesis of Ussami *et al.* (1986) - Profile 1

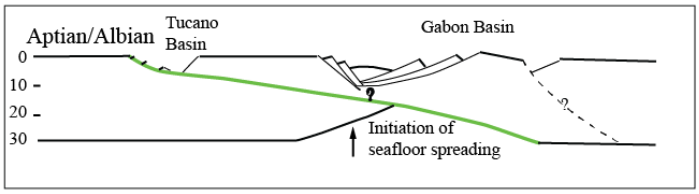

B) Hypothesis of Castro (1987) and Blaich et al. (2008) - Profile 2

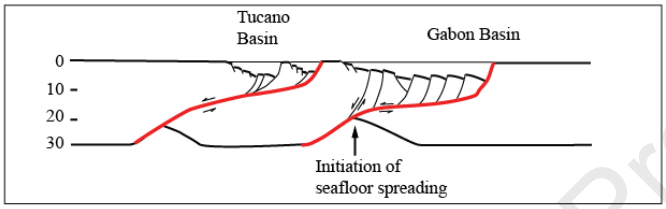

C) Hypothesis of Blaich (2006) - Profiles 2

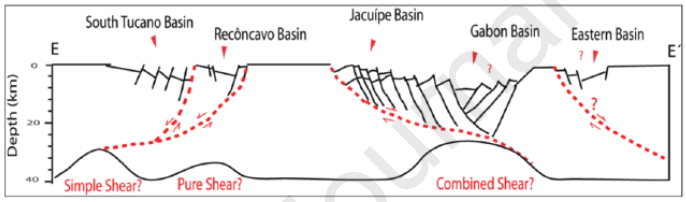

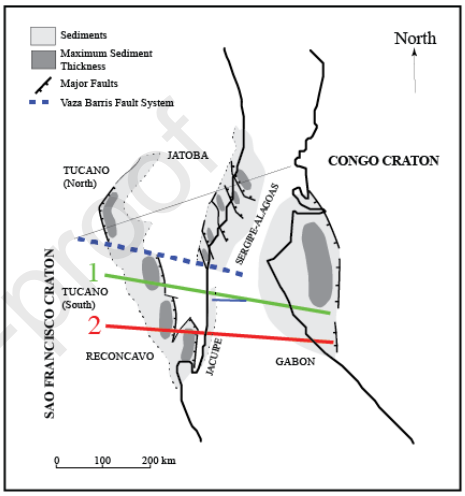

FIGURE 3

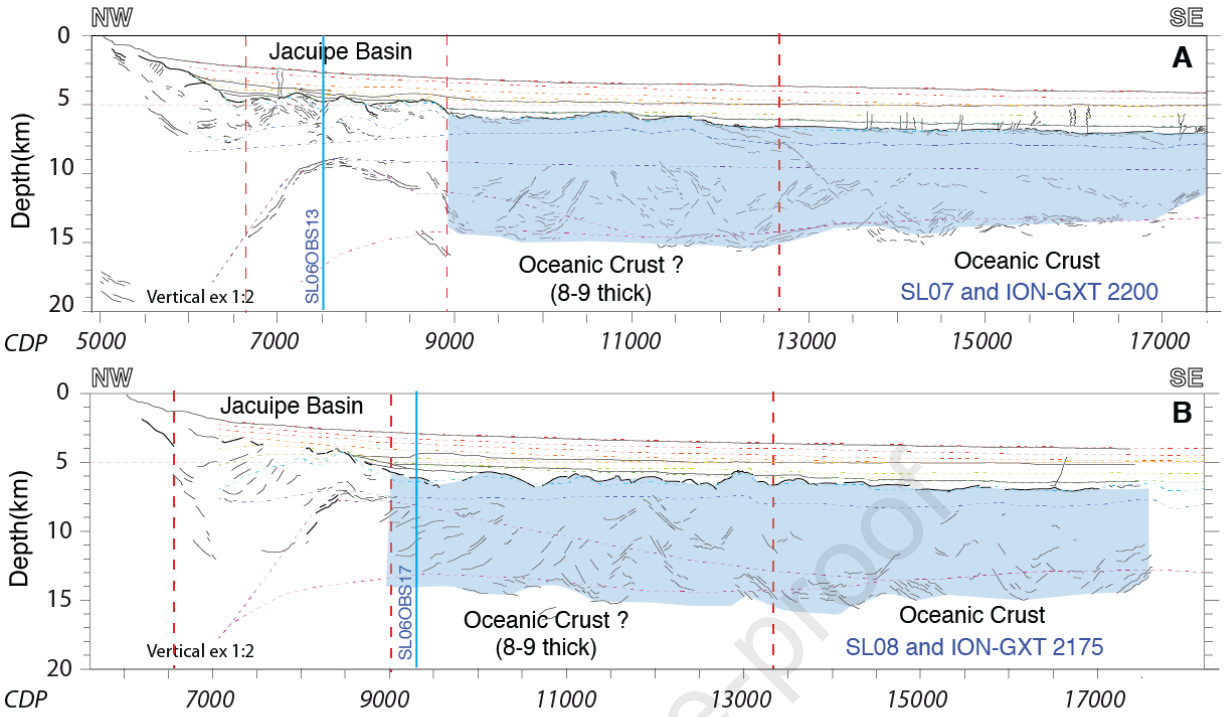

Figure 4

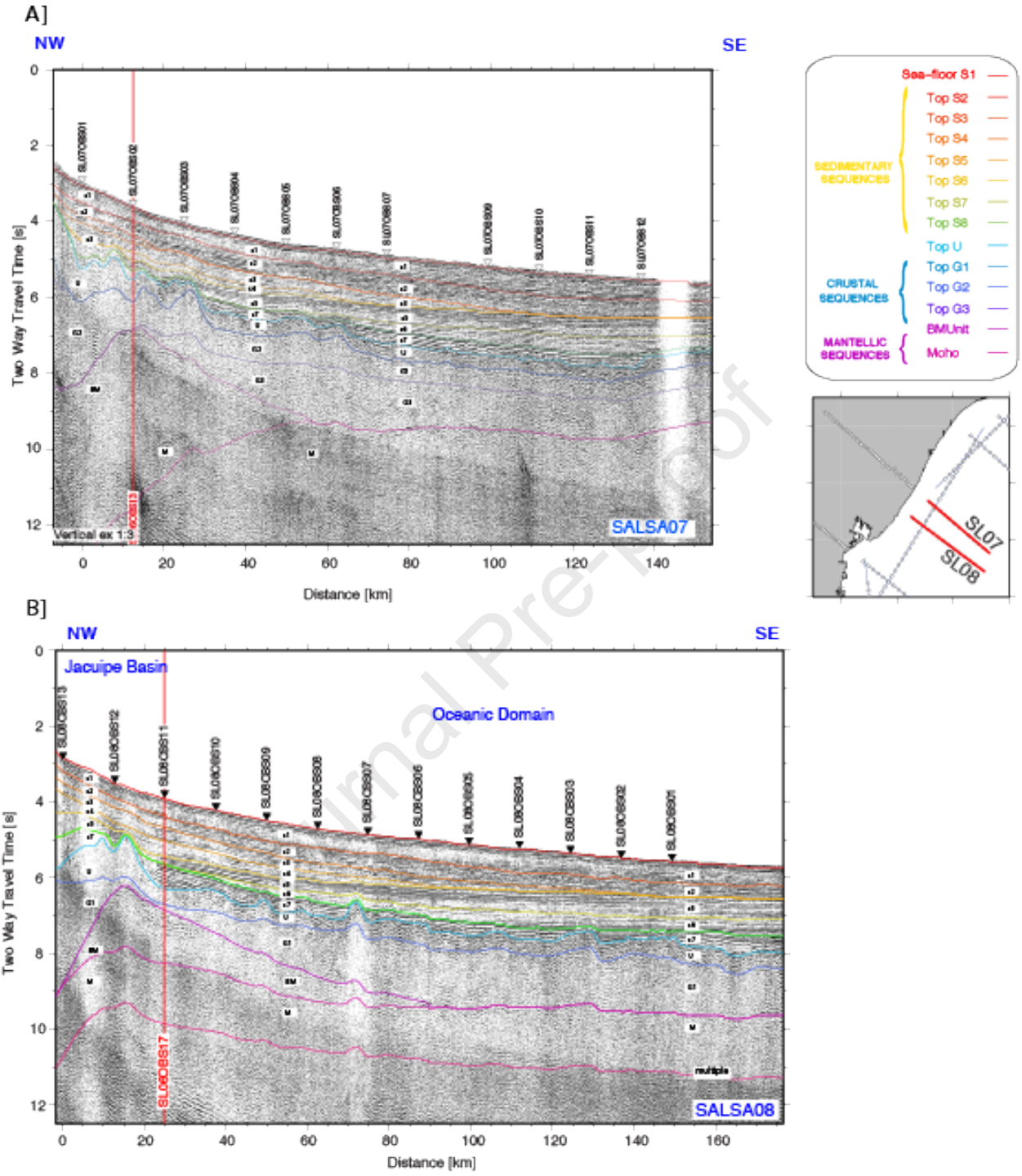
A]
NW
SE
Two Way Travel Time [s]
Distance [km]
Vertical ex 1:3
SALSA07
Sea-floor S1
Top S2
Top S3
Top S4
Top S5
Top S6
Top S7
Top S8
SEDIMENTARY SEQUENCES
Top U
Top G1
Top G2
Top G3
CRUSTAL SEQUENCES
BMUnit
MANTELLIC SEQUENCES
Moho
SL07
SL08
B]
NW
SE
Jacuipe Basin
Oceanic Domain
Two Way Travel Time [s]
Distance [km]
multiple
SALSA08

FIGURE 5

This study is part of the SALSA project (**S**ergipe **AL**agoas **S**eismic **A**cquisition), conducted by IFREMER (France) and Petrobras (Brazil), in collaboration with the CNRS (France), the Universidade de Brasilia (Brazil), the Faculdade de Ciências da Universiade de Liboa (Portugal) and the Université de Bretagne Occidentale (France).

During the SALSA cruise (2014), new geophysical and geological data were acquired (bathymetry, water column, sub-bottom profiler, gravity, magnetism, wide angle and reflection seismic) with 219 deployments of Ocean Bottom Sismometers over twelve wide-angle seismic on Pará-Maranhão/Barreirinhas passive margin in the Equatorial Atlantic segment. Simultaneously, Land Seismic Stations (LSS) were deployed along the Northeast Brazilian coast, extending five of those profiles on land for about 100 km in order to provide information on the onshore-offshore transition.

The SALSA project followed two previous projects with the same collaboration and same methodology: the SANBA project, devoted to structure and the geodynamic of the Santos Basin, and the MAGIC project, focused on the Ceara-Maranhão margins.

This article focuses on the two E-W marine seismic reflection and refraction data, SL07 and SL 08, that have been acquired using 15 and 13 ocean-bottom-seismometers along each profile, offshore the Jacuipe Basin. The SL07 has a 270-km long inland continuation with 46 land-seismic-stations crossing the South Tucano and Reconcavo Basins.

Briefly, the manuscript presents a strong E-W-segmentation with :

- A very abrupt necking zone
- An intermediate domain with anomalously high crustal velocities interpreted as intruded lower continental crust
- a sharp continent to ocean transition zone, greatly different from the adjacent segments.
- Below the Tucano half-grabens, the moho shows no rise, displaying a flat reflector throughout the landward part of the profile. The high seismic velocities areas in the lower continental crust are interpreted as intrusions that provide an overloading allowing the necessary subsidence for the deposition of the thick sedimentary basins

Together with the recent information given by continental basins and aborted rifts and similar wide-angle experiments on other margins and geodynamic contexts, we propose new paradigm for the thinning process which confirms the crucial role of the lower continental crust and its relation with the upper mantle, with a phase of overloading of the lower continental crust, an exhumation phase of the lower continental crust and a phase of proto-oceanic crust which involved the lower continental crust and the upper mantle, before a more typical oceanic crust.

Declaration of interests

☒ The authors declare that they have no known competing financial interests or personal relationships that could have appeared to influence the work reported in this paper.

☐ The authors declare the following financial interests/personal relationships which may be considered as potential competing interests: